POSITRON ANNIHILATION IN SINGLE CRYSTALS OF COPPER, ZINC, AND MAGNESIUM

by

EUGENE M. D. SENICKI

B.Sc., University of Manitoba, 1964

M.Sc., University of Manitoba, 1969

A THESIS SUBMITTED IN PARTIAL FULFILMENT OF THE REQUIREMENTS FOR THE DEGREE OF DOCTOR OF PHILOSOPHY

in the Department

of

PHYSICS

THE UNIVERSITY OF MANITOBA

February, 1972

ABSTRACT

A point geometry angular correlation apparatus for the study of positron annihilation in metals has been constructed. The apparatus achieves a high coincidence counting rate and is applicable to the study of all metals and alloys.

Angular distributions of the annihilation radiation from annealed single crystals of copper, zinc, and magnesium have been measured. The results are compared with the predictions obtained using a Wigner-Seitz type of calculation for the positron wavefunction and a more realistic calculation which takes the crystal symmetry of the wavefunction into account. The agreement between theory and experiment is considerably improved in the case of magnesium by the use of an enhancement factor.

ACKNOWLEDGEMENTS

The writer wishes to express his thanks to Dr. B. G. Hogg for his interest, guidance and encouragement during the period of this study. Thanks are also due to Dr. E. H. Becker, Dr. R. N. West and Mr. A. G. Gould for their valuable advice and discussions during the course of the experiments.

The writer also wishes to thank the Whiteshell Nuclear Research Establishment (AECL) for the use of the rabbit facilities and for making space available for the construction of the experimental apparatus. Without their kind cooperation this thesis would not have been possible.

Finally, the writer wishes to express his appreciation of the financial support given him during the course of this work. The research was supported by a grant from the National Research Council of Canada to Dr. B. G. Hogg.

TABLE OF CONTENTS

LIST OF FIGURES

LIST OF TABLES

LIST OF PLATES

CHAPTER 1

GENERAL INTRODUCTION

The positron, which had been predicted by Dirac in 1930, was first observed experimentally by Anderson in 1932 in cloud chamber photographs of cosmic ray showers. The existence of a bound state between the positron and an electron was first suggested by Mohorovicic in 1934 and the simplest and longest-lived, e^+e^- was named "positronium" by Ruark in 1945. The existence of the "atom" of positronium was experimentally confirmed in 1951 by Deutsch and soon the positron was being used as a tool in the investigation of matter.

Positron research may be divided into three categories:

1.) positronium physics

2.) positronium chemistry

3.) positron annihilation in metals

This thesis will be concerned with the third category where a clear and detailed theoretical understanding has not, at the present time, evolved.

When a positron annihilates with an electron, the most probable process is annihilation at rest with the emission of two photons in opposite directions each with energy m_0c^2. For an isolated system of a positron and an electron with opposite spins (singlet), an even number

(two or more) of photons must be emitted while, for the case of parallel spins (triplet), an odd number (at least three) of photons must be emitted. Zero or single quantum annihilation is possible in nonisolated systems but these are rare events. If positronium is formed, it will likely be in its ground state consisting of singlet and triplet before annihilating.

Normally two types of experiments are performed. One involves the measurement of the lifetime of the positron before annihilation while the other measures the angular correlation of the two photons emitted after annihilation. The experimental technique is that of the nuclear physicist using devices employed in gamma-ray spectroscopy and coincidence counting.

The lifetime experiments (2 gamma) measure the time delay between the entry of the positron into the sample signaled by a 1.27 MeV nuclear photon if the positron source is ^{22}Na and the appearance of the 0.511 MeV annihilation photon. The sample may be solid, liquid, or a gas. The curve of the coincidence rate vs. the time delay is then analyzed to give the lifetime of the positron in the system.

The lifetimes measured in metals are nearly constant and of the order of 0.2 nsec. Free positronium has a lifetime of about 0.12 nsec in the singlet state and about 0.1 μsec in the triplet state. A long lifetime of weak intensity has been measured in some metals giving a value of

around 1 nsec but this lifetime appears to be an anomaly of sample preparation rather than the result of positronium formation in the metal. There are few three gamma coincidences from metal samples. The situation in other solids and in liquids is complicated with numerous lifetimes measured between several tenths of a nsec and several hundred nsecs.

The angular correlation experiments measure the number of 2 photon coincidences as a function of the angle between the two photons. The angle is a measure of the center of mass momentum of the annihilating electron-positron pair. The maximum angle between the two photons is ~ 20 mrad.

The positron, after entering the metal sample, is nearly thermalized and so the main contribution to the momentum of the annihilating pair comes from the electron. The instrument, therefore, determines what is nearly the momentum distribution of the electron in the sample.

In a crystal, the conservation of momentum which gives the momentum of the annihilating pair in terms of the resulting photons is complicated by the Umklapp process where states corresponding to wave vectors differing by reciprocal lattice vectors are identical.

Up to this point in time, the best theoretical explanation of the data for metals is based on the independent particle model where the positron propagates in the medium under the influence of an averaged Hartree field. The method uses orthogonal-plane-wave (OPW) and augmented-plane-wave

(APW) methods for the calculation of conduction electron wave functions.

Many-body effects may, to a large extent, be neglected in the interpretation of angular distribution curves. The nonformation of positronium in metals is indicated in the angular correlation data by the absence of a narrow component.

This present work is a study of the annihilation of positrons in single crystals of copper, zinc and magnesium. The aim of the experiment is to critically test the independent particle theory of positron annihilation in metals, particularly with respect to the core electron contribution to the angular distributions where agreement between theory and experiment is not particularly good. A high resolution point geometry apparatus is described and the method is compared with other methods involving other geometries.

A less frequently employed technique involves the measurement of triple coincidence counting rates for three photon annihilations. This technique compliments the previous two described above. For further details of the interaction of positrons with matter in general, the reader is referred to the review articles by Ferrell (1956) and Wallace (1960) and to review articles in Stewart and Roellig (1967).

CHAPTER 2

POSITRON ANNIHILATION IN METALS

A. EXPERIMENTAL INTRODUCTION

The connection between the angular correlation of the two gamma rays emitted in positron annihilation and the electron momentum in solids was first made by DeBenedetti et al in 1949 and since then has been applied to various substances. The earlier work in metals (and semimetals) showed that the angular distributions could be divided into two groups (Stewart in Stewart and Roellig, 1967). The first group consists of those metals in which the angular distribution drops sharply to zero at a certain momentum and the second group in which there is no sharp drop. The first group is comprised of the following:

Li, Na, K, Rb, Cs, Mg, Ca, Sr, Zn, Cd, Al, Ga, In, Tl, Si, Ge, Sn, Pb

The second group consists of the following:

Cu, Ag, Au, Hg, B, C (graphite), Sb, Ti, V, Cr, Mn, Fe, Co, Ni, Rh, Pd, W

Be and Ba may belong to either group.

The first group is thought to correspond to those metals in which annihilations occur with mainly conduction electrons and the fairly sharp cutoff corresponds to the Fermi surface of the conduction electrons as calculated by

the free electron approximation. In the case of the alkali metals, where a free electron approximation would be expected to give reasonable results, the shape of the distributions are quite consistent with a spherical Fermi surface. The radii of the the spheres are in fairly good agreement with the values calculated from the free electron theory.

The situation is obviously more complicated in the second group of metals where the distributions extend well beyond the expected Fermi cutoff and do not show any breaks. This broad or gaussian part of the angular distribution is assumed to be due to annihilations with inner shell or core electrons. The possible existence of higher momentum components in the positron and electron wave functions resulting from the lattice potential may also take part in determining the shape of the angular distributions.

Positron annihilation, therefore, seems to be a tool for studying the Fermi surface in metals. With our present level of theoretical understanding and technical achievement, however, the method is somewhat limited. It is, nonetheless, of great importance to pursue a fundamental understanding of positron annihilation in metals. Positron annihilation experiments are one of the few sources of information about electrons which lie within the Fermi surface. Most of the other methods of checking the one-electron band theory and the electron gas many-body theory only involve the electrons at the Fermi surface. The method

does not require very low temperatures or high purity as do most of the other methods. This makes the method useful in the study of alloys where most of the electronic structure has not yet been verified.

Other competing techniques involve measurements of soft x ray emission (Fabian, 1968), Compton scattering (Phillips and Weiss, 1969), optical reflectivity (McAlister and Stern, 1965), photoemission, and neutron diffraction studies (Stedman and Nilsson, 1965).

PRINCIPLE OF MEASUREMENT

In the discussion of the detector geometries that follows it is assumed for convenience that the positrons annihilate in an electron gas and effects due to the crystal lattice are ignored.

When a positron annihilates with an electron in an electron gas, the center-of-mass momentum of the two particles appears as a small deviation from collinearity of the two gamma rays. This deviation can be detected. Let θ be the angle between the gamma rays. Conservation of momentum and energy gives θ as $|\underline{P}|/m_0 c$ where $\underline{P}$ is the sum of the momenta of the two photons, m_0 is the rest mass of the electron and c is the velocity of light. The positron is assumed to be nearly thermalized before annihilation so that $\underline{P}$ is nearly equal to $\underline{k}$ (apart from a factor $\hbar$), the momentum of the annihilating electron. The angle θ is typically of the order of several milliradians.

1.) LINEAR SLIT METHOD

The linear (long, wide) slit geometry introduced by Lang and DeBenedetti (1957) is the most common method used in angular correlation experiments. This is a result of the limited strength of available positron sources (a few mC of ^{22}Na is commonly used) and the small effective solid angle required in the determination of the correlation. The resulting coincidence counting rates are low and so there must be a compromise between good resolution and small statistical uncertainties in counting.

The positron source is placed close to a sample which is viewed by two photomultiplier detectors. The photons are collimated by long and narrow slits. By moving one of the detectors while keeping the other fixed, we are able to measure the coincidence count rate as a function of the displacement of the moveable detector. This geometry only measures the projection on the yz plane of the angle between the photons. The detector is moved through ~ ± 20 mrad while typical values for slit widths are ~ 0.1 cm; slit lengths ~ 10 cm; sample length ~ 2 cm; sample to detector distance ~ 200 cm. The z component of θ is given by $\theta=z/d$ where z is the displacement of the moveable detector from the xy plane and d is the distance between the sample and the detector. This results in the relation $P_z = m_0 cz/d$.

The coincidence counting rate as a function of P_z is given by

$$N(P_z) \propto \int_{-\infty}^{\infty} dP_x \int_{-\infty}^{\infty} dP_y \; \rho(\underline{P}) \qquad (2\text{-}1)$$

where $\rho(\underline{P})$ is the density of annihilating pairs of gamma rays or equivalently the density of electronic states of the electron gas in momentum space. The integration to infinity in the P_x is justified by the fact that the slits are much longer than the length corresponding to the Fermi radius. P_y can be integrated to infinity since the detectors accept a larger range of energies than the spread due to the Doppler shift caused by the kinetic energy of the electron (Hotz et al, 1968).

Since $\rho(\underline{P})=0$ outside the Fermi surface (a sphere of radius $\hbar k_F$ in the case of a free electron gas) and is constant inside, the coincidence count rate with $P_z=m_0 c\theta$ is proportional to the area of a slice through the Fermi surface perpendicular to the P_z axis, intercepting the P_z axis at $m_0 c\theta$. Thus from Figure 1

$$N(P_z) \propto [\hbar^2 k_F^2 - (m_0 c\theta)^2]$$

or taking $\hbar k_F = m_0 c\theta_F$,

$$N(P_z) \propto (\theta_F^2 - \theta^2) \qquad (2\text{-}2)$$

The expected angular distribution for a free electron gas in the long slit geometry is, therefore, a parabola centered at $\theta = 0$ and intercepting the θ axis at θ_F. The value of the intercept θ_F gives the radius of the Fermi surface. Differences between the free electron parabola and the curve obtained for real metals arise because the Fermi surface is different from a sphere and higher momentum components due to the lattice potential may contribute. The positron also

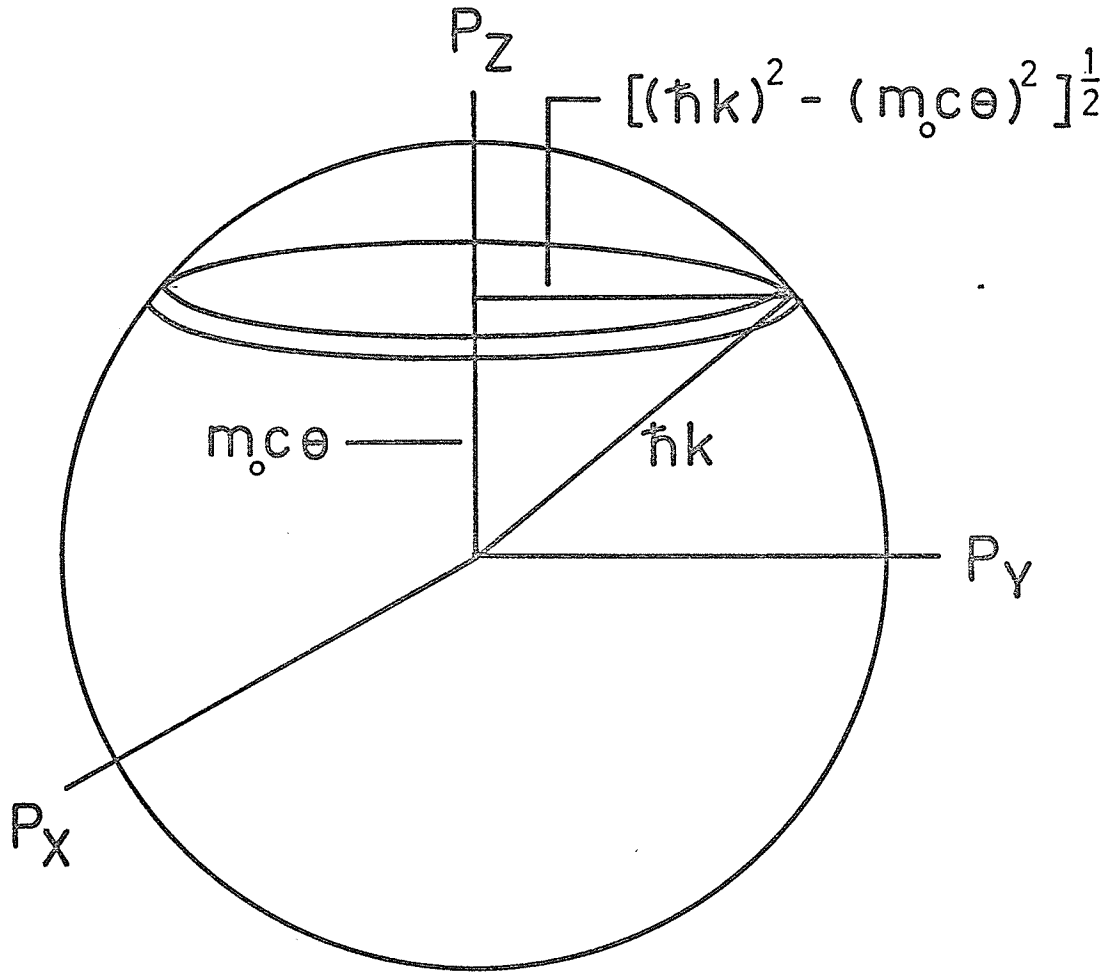

Figure 1. Region sampled by the linear slit geometry.

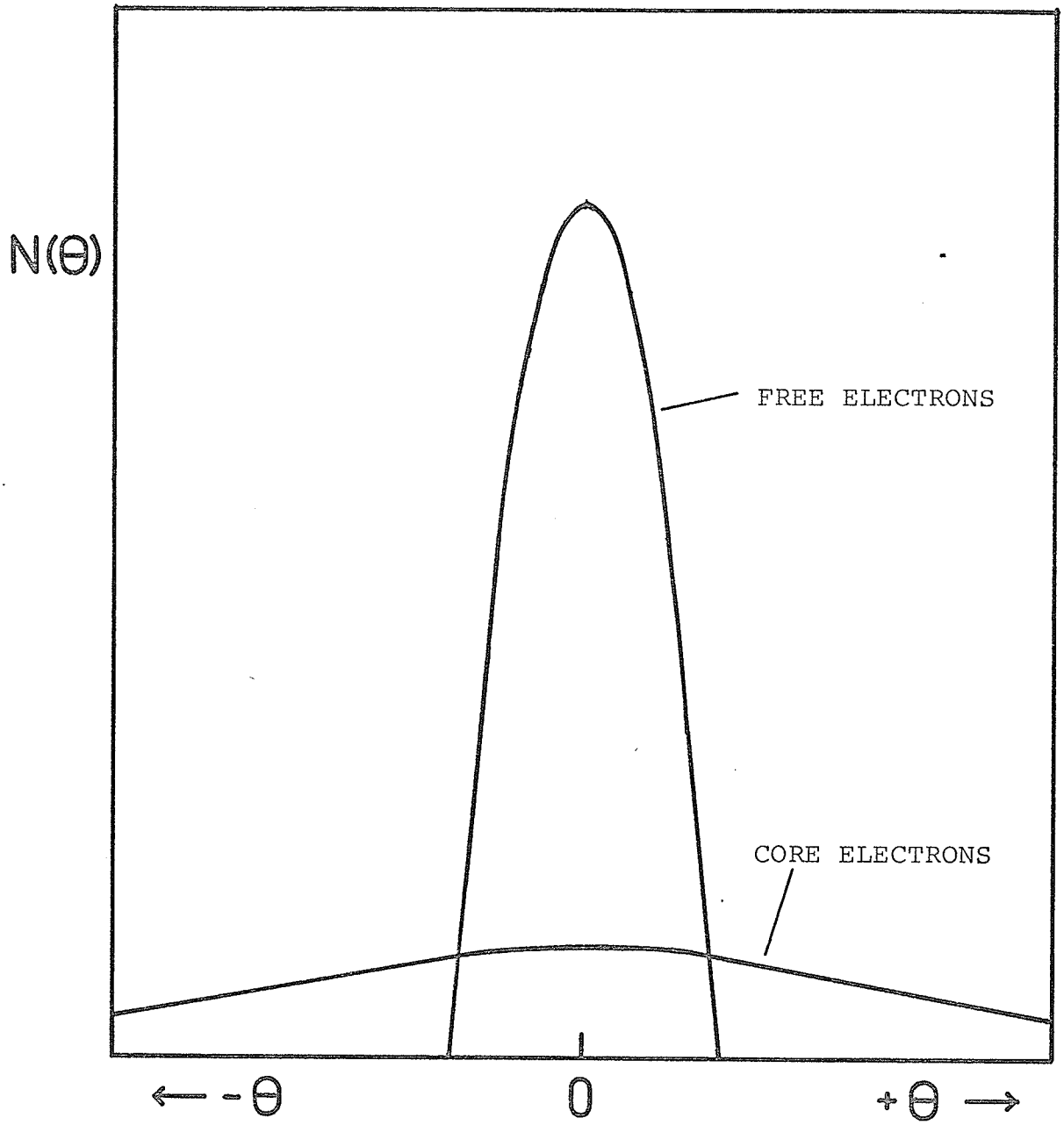

Figure 2. The expected angular distribution for free and core electrons in the linear slit geometry.

annihilates to a lesser extent with core electrons and this contribution, which is usually rather broad and smoothly varying, obscures the position of the Fermi cutoff. The expected distribution for free electrons and core electrons is shown in Figure 2.

2.) POINT SLIT METHOD

This geometry was originally introduced by Colombino et al (1963). In this geometry, the long and narrow slits of the previously discussed geometry are replaced by circular holes roughly equal to the width of the narrow slits. The solid angle subtended by the detectors at the sample is now substantially smaller than the solid angle subtended in a typical long slit experiment and the resulting coincidence counting rate is greatly reduced. The coincidence counting rate is given by

$$N(P_z) \propto \int_{-\infty}^{\infty} \rho(0,P_y,P_z)\,dP_y \qquad (2\text{-}3)$$

We see from Figure 3 that the region of the Fermi surface sampled is now a cylinder rather than a slice, as in the long slit geometry, and we have

$$\begin{aligned} N(P_z) &\propto [\hbar^2 k_F{}^2 - (m_0 c\theta)^2]^{\frac{1}{2}} \\ &\propto (\theta_F{}^2 - \theta^2)^{\frac{1}{2}} \end{aligned} \qquad (2\text{-}4)$$

The angular distribution for free electrons in this geometry is a circle of radius $\sim \theta_F$. Experimentally, the procedure is the same as for the long slit geometry. One detector is moved sideways and successive chords of the sphere are measured. Departures from a spherical

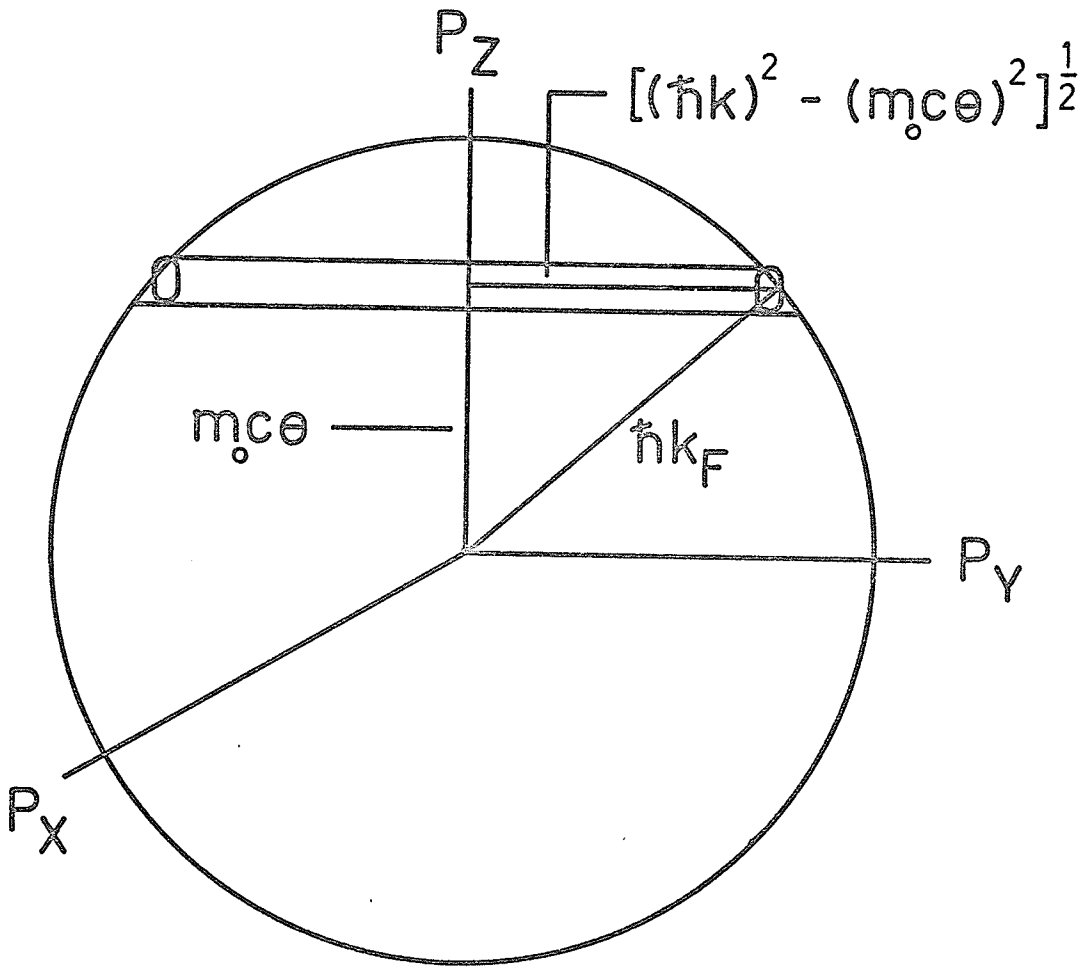

Figure 3. Region sampled by the point slit geometry.

Fermi surface result in a deviation from the form indicated in the expression for $N(P_z)$ and we expect a cutoff at θ_F obscured by core annihilations.

Alternatively, the detectors can be fixed at the collinear position ($\theta=0$), and the coincidence rate can be recorded as a function of the crystal orientation. Equation (2-4) gives the result that at $\theta=0$ the coincidence rate is proportional to the radius of the Fermi surface. This technique has been termed the collinear or rotating specimen method (Williams et al, 1968; Sueoka, 1967). The method takes advantage of the high counting rate at $\theta=0$ and reflects the details of the Fermi surface more sharply than the angular correlation method. The method cannot, however, give the absolute size of the Fermi surface nor the contribution of the core electrons in a direct way and it relies on the angular correlation method to obtain this information.

In general, the point slit geometry offers some distinct advantages over the long slit geometry. One advantage is that features due to the Fermi surface may be smeared out by the averaging that occurs in the long slit geometry in taking a slice through the Fermi surface and these features may be observed with the point geometry where the counting rate is proportional to a chord through the Fermi surface. The smearing due to higher momentum components in the electron and positron wavefunctions is less in the point geometry since more higher momentum components are likely to fall inside a slice than in a cylinder. Similarly,

the ratio of core electron to conduction electron contribution is less for the point geometry and so the point geometry is better suited to the study of metals with large core contributions.

The point slit geometry has been used by Colombino et al (1963) and (1964), and Williams et al (1968).

3.) CROSSED SLIT METHOD

This method is a compromise between the two previously discussed geometries. It is essentially the same as the long slit method except that the length of the slits is reduced to a certain extent comparable to the length corresponding to the Fermi surface of copper. This method was introduced by Fujiwara and Sueoka (1966) and is used primarily by that group in both the angular correlation and rotating specimen experimental modes.

B. THEORETICAL INTRODUCTION

THE INDEPENDENT PARTICLE MODEL

In this model, we ignore any interactions between the positron and the valence electrons and between the valence electrons themselves due to their Coulomb repulsion. Such effects in the core, or between core and valence electrons are treated as part of the potential seen by the positron and each valence electron as they move through the metal crystal. The potential is calculated as a Hartree or Hartree-Fock potential of the ion.

The annihilation process proceeds by an intermediate state in which the electron and positron are still present and one photon has been created. The pair then annihilates emitting a second photon. The matrix element for the process is of the form (Ferrell, 1956)

$$\int_V \Psi_+(\underline{r})\Psi_-(\underline{r})e^{-i\underline{P}\cdot\underline{r}}\, d^3\underline{r} \qquad (2\text{-}5)$$

where $\underline{P}$ is the momentum of the annihilating pair and $\Psi_+(\underline{r})$ is the wavefunction of the positron and $\Psi_-(\underline{r})$ is the wavefunction of the electron. The electronic momenta of the intermediate states are much greater than those of the initial and final states. The matrix element for the process is then nearly independent of the momentum of the initial state.

For an electron with wave vector $\underline{k}$ annihilating with a positron, the probability of the two photons carrying net momentum between $\underline{P}$ and $\underline{P} + d\underline{P}$ is given by

$$\rho_{\underline{k}}(\underline{P})\,d^3\underline{P} \propto \left| \int_V \Psi_+(\underline{r})\,\Psi_{\underline{k}}(\underline{r})\,e^{-i\underline{P}\cdot\underline{r}}\,d^3\underline{r} \right|^2 d^3\underline{P} \qquad (2\text{-}6)$$

The total annihilation rate is obtained by summing over the occupied states $\underline{k}$ and integrating over all momenta and is given by

$$\lambda = \sum_{\underline{k}_{occ}} \int \rho_{\underline{k}}(\underline{P})\; d^3\underline{P} \qquad (2\text{-}7)$$

The mean life of the positron is $\bar{t} = \lambda^{-1}$.

THE THERMALIZATION OF POSITRONS IN METALS

Initially, the positron has several kilovolts of energy when it enters a metal. The positron then loses energy rapidly by the creation of electron-hole pairs until it reaches equilibrium with its surroundings. The positron then has an energy of the order of kT where k is the Boltzmann constant and T is the absolute temperature of the surroundings before annihilation.

Estimates of the thermalization time have been made by Garwin (1953) and Lee-Whiting (1955) and more recently by Carbotte and Arora (1967). Lee-Whiting used ordinary perturbation theory with a screened Coulomb potential of the form $(e^2/r)e^{-\lambda r}$ where λ is a semi-phenomenological screening parameter and r is the distance between the positron and the valence electron. He obtained for the lifetime before annihilation a value of about 100 times the thermalization time for Na at room temperature.

The smallness of the thermal energy of the positron (0.05 eV at room temperature) as compared to the electronic energy of the system ($E_F \sim 5$eV) means that the positron

annihilates from a state of zero crystal momentum.

The result of Carbotte and Arora was based on a Green's function approach to the problem. The main difference was that their value for λ was the Thomas-Fermi value. They arrived at the conclusion that at low temperatures the positron may not be thermalized. The positron energy, however, is still of the order of 0.1 eV in a time very much shorter than the lifetime before annihilation.

BAND THEORY

In a real metal, the electron and positron can be represented by Bloch functions

$$u_{\underline{k}}(\underline{r})\, e^{i\underline{k}\cdot\underline{r}} \tag{2-8}$$

where $u_{\underline{k}}(\underline{r})$ is periodic with period $\underline{\ell}$, the lattice vector of the crystal. The function $u_{\underline{k}}(\underline{r})$ is of the form

$$u_{\underline{k}}(\underline{r}) = \sum_{\underline{G}} a_{\underline{G}}(\underline{k})\, e^{i\underline{G}\cdot\underline{r}} \tag{2-9}$$

where $\underline{G}$ is a reciprocal lattice vector. This will introduce higher momentum components into the positron and electron wavefunctions which are plane waves for free particles. Since the positron is thermalized we have $\underline{k} = \underline{0}$ for the positron.

The momentum distribution can then be written[†]

$$\rho_{\underline{k}}(\underline{P}) \propto \left| \int_{\text{crystal}} \psi_+(\underline{r})\, u_{\underline{k}}(\underline{r})\, e^{i(\underline{k}-\underline{P})\cdot\underline{r}}\, d^3\underline{r} \right|^2 \tag{2-10}$$

where $\psi_+(\underline{r})$ and $u_{\underline{k}}(\underline{r})$ are periodic with the periodicity of the lattice.

---

† Atomic units (a.u.)

CALCULATION OF THE POSITRON WAVE FUNCTION

$\psi_+(\underline{r})$ can be calculated using the Wigner-Seitz method where ψ_+ is calculated subject to the condition $(\psi_+)' = 0$ on the sphere $r = r_S$ where $\frac{4}{3}\pi r_S^3$ is the volume of the Wigner-Seitz sphere. $(\psi_+)' = \frac{\partial}{\partial r}\psi_+$.

The diameters of the orbits of the core electrons are smaller than the distance of the atoms apart, so that the charge in one cell is due to the ion and to the valence electrons in that cell. To a high degree of approximation the charge distribution is spherically symmetrical, and the charge in any cell produces zero electric force at points outside the cell. ψ_+ is calculated, therefore, as the solution of the Schrödinger equation with a potential due to the metal ion at the center of the cell plus a free electron gas inside the cell. The potential due to the ion is known numerically from selfconsistent field calculations.

Inside the cell centered at the origin, $\psi_+ = R_+(\underline{r})/r$ and R_+ satisfies (in a.u.)

$$R_+'' + [E+2V(r)]R_+ = 0. \qquad (2\text{-}11)$$

This equation is solved numerically by determining a spherically symmetrical solution starting from the origin and E is chosen to fit the boundary condition $(R_+/r)' = 0$ at $r = r_S$.

ψ_+ can also be calculated by expanding the wave-function as a Fourier series

$$\psi_+(\underline{r}) = \sum_{\underline{G}} c_{\underline{G}}\, e^{i\underline{G}\cdot\underline{r}} \qquad (2\text{-}12)$$

and similarly for the potential, V

$$V(\underline{r}) = \sum_{\underline{G}} V_{\underline{G}}\, e^{i\underline{G}\cdot\underline{r}} \qquad (2\text{-}13)$$

where $\underline{G}$ is a reciprocal lattice vector. Substituting these into the Schrödinger equation results in an infinite set of linear equations for the $c_{\underline{G}}$'s:

$$\sum_{\underline{G}} \left[(G^2-E)\delta_{\underline{G},\underline{G}'} + V_{\underline{G}'-\underline{G}}\right] c_{\underline{G}} = 0. \qquad (2\text{-}14)$$

A solution can only exist if the secular determinant vanishes. The potential is, as before, the potential of a Hartree-Fock core plus a free electron gas. The equations are solved numerically for the ground state value of E and the coefficients $c_{\underline{G}}$.

ANNIHILATION WITH CORE ELECTRONS

The core electrons can be treated in the tight-binding approximation in which

$$u_{\underline{k}}(\underline{r})\, e^{i\underline{k}\cdot\underline{r}} = \sum_{\underline{\ell}} e^{i\underline{k}\cdot\underline{\ell}}\, \phi(\underline{r}-\underline{\ell}) \qquad (2\text{-}15)$$

and $\phi(\underline{r})$ is a normalized atomic wavefunction.

The momentum distribution for core electrons is, therefore, given by

$$\rho_{\underline{k}}(\underline{P}) \propto \left| \sum_{\underline{\ell}} e^{i(\underline{k}-\underline{P})\cdot\underline{\ell}} \int_{\text{crystal}} \psi_+(\underline{r})\,\phi(\underline{r})\, e^{-i\underline{P}\cdot\underline{r}}\, d^3\underline{r} \right|^2$$

$$\propto \delta[\underline{k} + \underline{G} - \underline{P}] \left| A_{\underline{G}}(\underline{k}) \right|^2 \qquad (2\text{-}16)$$

where

$$A_{\underline{G}}(\underline{k}) = \int_{\text{crystal}} \psi_+(\underline{r})\,\phi(\underline{r})\,e^{-i(\underline{k}+\underline{G})\cdot\underline{r}}\,d^3\underline{r} \qquad (2\text{-}17)$$

If we have a full zone, it will always be possible to find a $\underline{G}$ such that $\underline{P} - \underline{G}$ is in the occupied region and as a result the total momentum is given by

$$\rho_\phi(\underline{P}) \propto \sum_{\underline{G}} \left| A_{\underline{G}}(\underline{P} - \underline{G}) \right|^2 \qquad (2\text{-}18)$$

ANNIHILATION WITH CONDUCTION ELECTRONS

In what follows we approximate the positron wavefunction as constant and write the electron wavefunction as a Bloch function.

If the coefficient $a_{\underline{G}}(\underline{k})$ is assumed to be independent of $\underline{k}$, the momentum distribution can be written as

$$\rho_{\underline{k}}(\underline{P}) \propto \left| \sum_{\underline{G}} a_{\underline{G}} \int_{\text{crystal}} e^{i(\underline{k}+\underline{G}-\underline{P})\cdot\underline{r}}\,d^3\underline{r} \right|^2$$

$$\propto \sum_{\underline{G}} \delta[\underline{k} + \underline{G} - \underline{P}]\ |a_{\underline{G}}|^2 \qquad (2\text{-}19)$$

The total momentum distribution is obtained by summing over the occupied states of $\underline{k}$:

$$\rho(\underline{P}) \propto \sum_{\underline{k}_{occ}} \sum_{\underline{G}} |a_{\underline{G}}|^2\ \delta[\underline{k} + \underline{G} - \underline{P}] \qquad (2\text{-}20)$$

The angular distribution in the point geometry is given by

$$N(P_z, P_x=0) \propto \int_0^\infty \rho(\underline{P})\ dP_y$$

$$\propto \int_{P_z}^\infty \rho(\underline{P})\ P[P^2 - P_z^2]^{-\frac{1}{2}}\ dP \qquad (2\text{-}21)$$

where $P = P_y^2 + P_z^2$. From equations (2-20) and (2-21), we find

$$N(P_z, P_x=0) \propto \sum_{\underline{G}} |a_{\underline{G}}|^2 \{k_F^2 - [(\underline{P}-\underline{G})_z^2 + G_x^2]\}^{\frac{1}{2}} \qquad (2\text{-}22)$$

where $\underline{P} - \underline{G}$ must lie in the occupied region of k-space.

In other words, the only "occupied" regions of momentum space are a set of nonoverlapping spheres (roughly) of radius k_F that are centered at reciprocal lattice points. In the point geometry, we cut through sets of spheres as we move one detector through an angle θ. Each sphere contributes an amount proportional to a chord through the sphere weighted by the factor $|a_{\underline{G}}|^2$. This is illustrated schematically in Figure 4 (the spheres in Figure 4 are assumed to lie in the yz plane).

Clearly, equation (2-22) depends on the shape of the Fermi surface. In simple metals, where the core contribution is small and isotropic and the Fermi surface is almost spherical, the contributions due to core electrons can be separated from the conduction electron contribution and the result can be interpreted in terms of the shape of the Fermi surface. If the coefficients are strongly k-dependent, an interpretation in terms of the shape of the Fermi surface is impossible and more advanced band structure calculations must be performed to obtain the wavefunctions for $\psi_+(\underline{r})$ and $\psi_-(\underline{r})$.

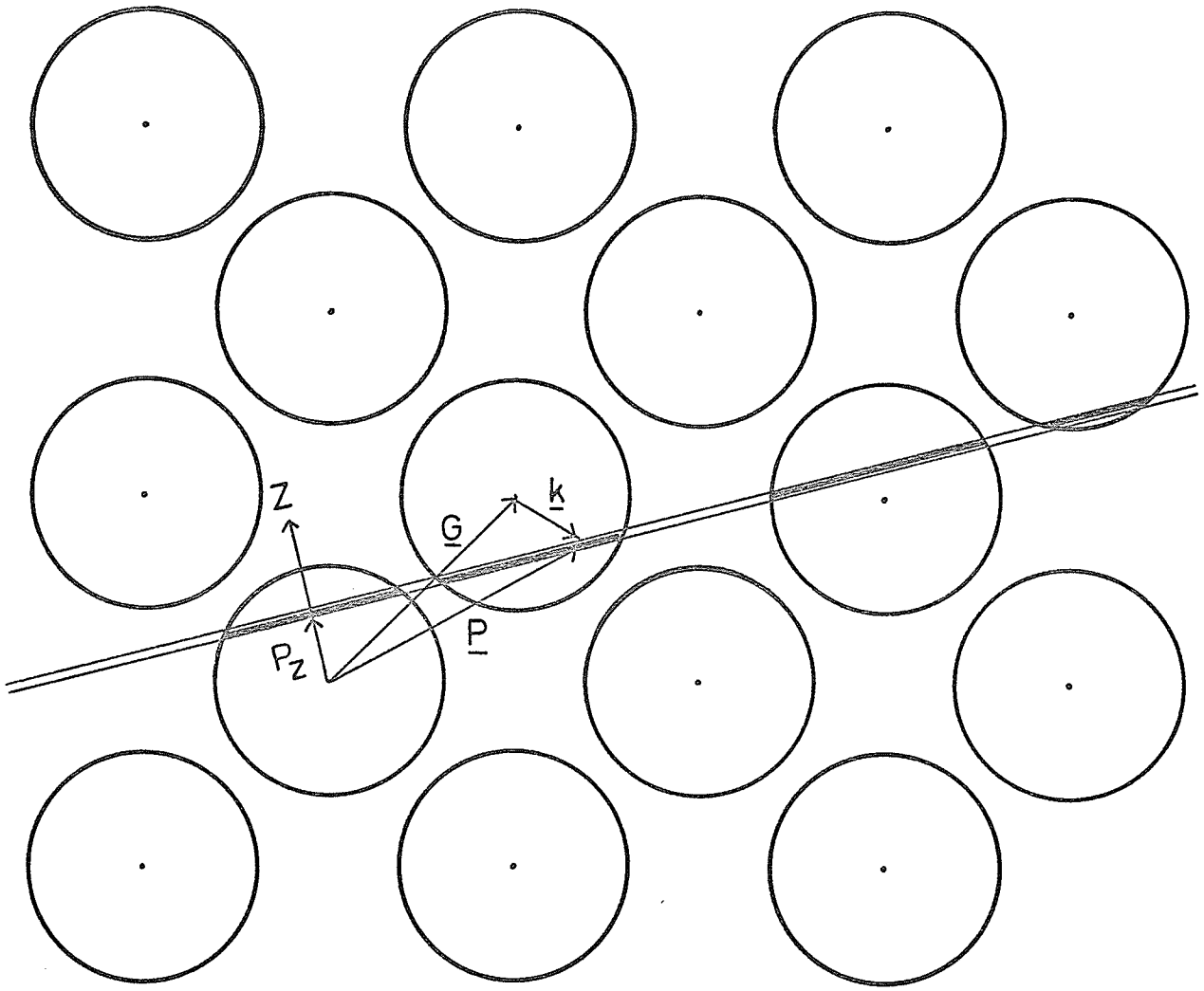

Figure 4. Schematic representation of Fermi surfaces situated at reciprocal lattice points indicating the region sampled by the detectors.

CALCULATION OF THE CONDUCTION ELECTRON WAVEFUNCTION

The function $u_0(\underline{r})$ can be calculated by the Wigner-Seitz method to be used in determining the momentum distribution for annihilation with conduction electrons near $\underline{k} = \underline{0}$.

The conduction electron contribution can also be considered to be due to the smooth part of the conduction electron wavefunction in an orthogonalized plane wave (OPW) calculation. This wavefunction is a Bloch function of the form of equation (2-8) and is the solution of a modified Schrödinger equation

$$[-\nabla^2 + V_P]\psi_{\underline{k}}(\underline{r}) = E_{\underline{k}}\psi_{\underline{k}}(\underline{r}) \qquad (2\text{-}23)$$

where V_P is a pseudopotential, or effective potential. V_P is expanded as a Fourier series

$$V_P = \sum_{\underline{G}} V_{\underline{G}} e^{i\underline{G}\cdot\underline{r}} \qquad (2\text{-}24)$$

and the resulting equation is

$$\sum_{\underline{G}} [(\underline{k}-\underline{G})^2 \delta_{\underline{G},\underline{G}'} - E_{\underline{k}} + V_{\underline{G}'-\underline{G}}] a_{\underline{G}} = 0. \qquad (2\text{-}25)$$

This equation is solved numerically for the $a_{\underline{G}}$'s.

THE ANGULAR CORRELATION STUDIES IN SINGLE CRYSTALS

The earlier measurements of the angular distributions of annihilation radiation from metals were performed on polycrystalline samples. This resulted in a determination of only the spherical average of the momentum distributions

of the valence electrons in these metals (Lang and DeBenedetti, 1957; Stewart, 1957). Berko et al (1957), in an experiment on oriented graphite, showed that momentum anisotropies in oriented single crystals could be measured. Several experiments have since been performed with the hope of obtaining information about the electron properties in metals and particularly the shape of the Fermi surface.

Measurements on single crystals of copper and aluminum were performed by Berko and Plaskett (1958) revealing little anisotropy for different crystal orientations. They discussed, in terms of the independent particle model, the importance of the positron wavefunction and several types of electron wavefunctions. In particular, they studied Wigner-Seitz positrons and tightly bound, nearly free and Wigner-Seitz electrons. They were able to show that the high momentum tail in the copper distribution was due to annihilation with the 3d electrons (core electrons). Their calculations were moderately successful in describing their experimental results, especially in aluminum which has a relatively small wide angle distribution when compared with copper. Their results showed that the one-electron theory could be used to account for the experimental observations in relatively great detail.

Angular correlation curves were measured for oriented beryllium and magnesium crystals by Berko (1962). Considerable anisotropy was observed in beryllium compared

to the nearly isotropic behavior of magnesium. The anisotropy in beryllium was interpreted as due to the effect of the Fermi distribution overlapping into the second zone (Berko and Plaskett, 1958) and deviations of the electron wavefunctions from plane waves. Since the effect of the overlapping depends on the energy gap in the band structure, the energy gap in beryllium was concluded to be larger than that of magnesium. The Fermi surface of magnesium was, therefore, very nearly spherical. The angular distribution of the annihilation radiation from beryllium was also measured by Stewart et al (1962) and showed the same appreciable anisotropy. The experiment was repeated by Shand and Stewart (1966).

It is very difficult to obtain the topology of the Fermi surface for real metals in a direct way. The cutoff corresponding to the Fermi surface is only roughly that corresponding to the actual Fermi momentum and the approximation that the counting rate is proportional to the area of a slice or the length of a chord through the Fermi surface seems to be inadequate. The angular correlations are quite sensitive to the form of the wavefunctions for the positron and the electron and it is necessary, therefore, to first postulate a Fermi surface and then proceed to calculate the experimental curve. The beryllium data of Shand and Stewart (1966) was analyzed by Shand (1969) who used a local pseudopotential model for the conduction

electrons chosen to fit the Fermi surface of beryllium. Using a constant positron wavefunction, he was able to reproduce the data reasonably well.

Donaghy and Stewart (1967) studied lithium in great detail in an attempt to determine a Fermi surface. They used "humps" in the [110] directions and higher momentum components in the electron wavefunction to obtain a fit to their data. They found a 5% deviation from sphericity in agreement with theoretical predictions. A complete band calculation using the orthogonalized-plane-wave method (OPW) for the conduction electron wavefunction and the Wigner-Seitz method for the positron wavefunction was performed by Melngailis and DeBenedetti (1966) and used to interpret the data of Donaghy and Stewart. They calculated the core contribution by assuming tight-binding functions for the core electrons. They obtained qualitively good agreement with experiment in predicting the anisotropies in the angular distribution curves. The agreement was improved by multiplying the theoretical curve by the free electron enhancement factor of Kahana (1963). They found that the anisotropies in the tail of the experimental curve could be explained by the anisotropy in the valence electron contribution. Their results were also quite sensitive to their choice of core electron wavefunction and the way in which the core contribution was subtracted. The experimental data has recently been reinterpreted by Stachowiak (1970)

using a method due to Mijnarends (1967, 1969). He found evidence for the possible existence of a neck in the Fermi surface in the [110] direction with a radius of the order of 13% of the free electron sphere radius.

The first calculation for a transition metal was performed by Loucks (1966) on yttrium oriented with the c axis in the z direction for the long slit geometry. The strong d-character of the valence states in transition metals makes an interpretation in terms of the shape of the Fermi surface impossible. This makes it necessary to perform a band structure calculation in order to interpret the data. Loucks discussed the theory of positron annihilation in terms of the independent particle model using the augmented-plane-wave method (APW). His calculation qualitatively explained the experimental results of Williams and Mackintosh (1966, 1968). The lack of structure in the experimental results which was predicted by the theoretical model was attributed to smearing due to Coulomb correlation effects.

The angular distributions of the annihilation radiation were calculated for yttrium and zirconium by Gupta and Loucks (1968) based on the APW method. The theory for yttrium predicted a more pronounced hump than the earlier calculation but with the same general shape. The angular distribution for zirconium was measured by Coussot (1971) and confirmed that at small angles, the curve falls below the free electron parabola. The experiment did not resolve

a small predicted hump near the zone boundary but indicated expected contributions due to the higher momentum components in the electron wavefunction.

Since the work of Berko and Plaskett (1958), there have been a number of attempts to relate the results of positron annihilation in copper single crystals with detailed features of the Fermi surface. The necks were first observed independently by Fujiwara (1965) (Fujiwara and Sueoka, 1967, Sueoka, 1967) and Williams et al (1965; 1968). Other experiments on copper single crystals were performed by Berko et al (1968), Mijnarends (1969), Murray and McGervey (1970), and Cushner et al (1970). These experiments were all interpreted in terms of the Fermi surface topology.

The Fermi surface of copper is distorted from a sphere to the extent that the Fermi surface makes contact with the (111) zone faces of the Brillouin zone. Using the nearly free electron approximation, Berko and Plaskett (1958) predicted a smearing of the transition between the peak and the tail of the experimental data due to higher momentum components, especially where the zone face is perpendicular to the z direction. Whether this occurs or not is still unsettled. The theory is confirmed by the results of Berko et al (1968) and Cushner et al (1970) and Mijnarends (1969) while the results of Fujiwara et al (1967) are in contradiction with the theory as are the results of Mogensen and Trumpy (1969) in tin and bismuth.

The most recent experiments in zinc single crystals were performed by Mogensen and Petersen (1969) and showed small anisotropies between different single crystal curves. Anisotropies were observed in the tails of the distributions. The results in tin and bismuth (Mogensen and Trumpy, 1969) were free-electron-like with the tin curves showing more anisotropy than the bismuth curves. There was evidence for anisotropy in the wide angle part of the curves as well.

Existing data for aluminum and silicon were analyzed by Stroud and Ehrenreich (1968) using pseudo-potential wavefunctions for the conduction electrons and realistic positron wavefunctions having the correct crystal symmetry. The positron wavefunction was calculated using potentials derived from x ray diffraction data. Their results were in surprisingly good agreement with the experimental data. The conduction electron contribution was sensitive to the shape of the positron wavefunction for silicon but less sensitive for aluminum. The results for the contribution outside the Fermi surface were quite strongly dependent on the shape of the positron wavefunction.

CHAPTER 3

DESCRIPTION OF THE EXPERIMENTAL APPARATUS

GENERAL ARRANGEMENT

The apparatus was constructed using the point detector geometry and is shown schematically in Figure 5. It consisted of basically eight NaI(Tl) scintillation detectors (only four are shown in Figure 5) connected to record coincidences between paired detectors (A and C in Figure 5 would be such a pair, for example). Four pairs of detectors were used in an attempt to rationalize the constraints of room size, counting rate and cost.

For rigidity, the entire apparatus was mounted on two 3-in x 6-in aluminum I-beams which were about 26 ft long. The I-beams were placed about 3 ft apart and rested on concrete blocks placed at about every 3 ft along their lengths. The detectors were mounted at opposite ends of the I-beams on platforms which were firmly bolted to the I-beams. A large electromagnet at the center of the apparatus rested on a steel plate which was firmly bolted to the bottom of the I-beams. A vacuum box which housed the positron source and metal sample to be studied was positioned between the pole-faces of the magnet. The distance between the detectors and the sample was 140-in .

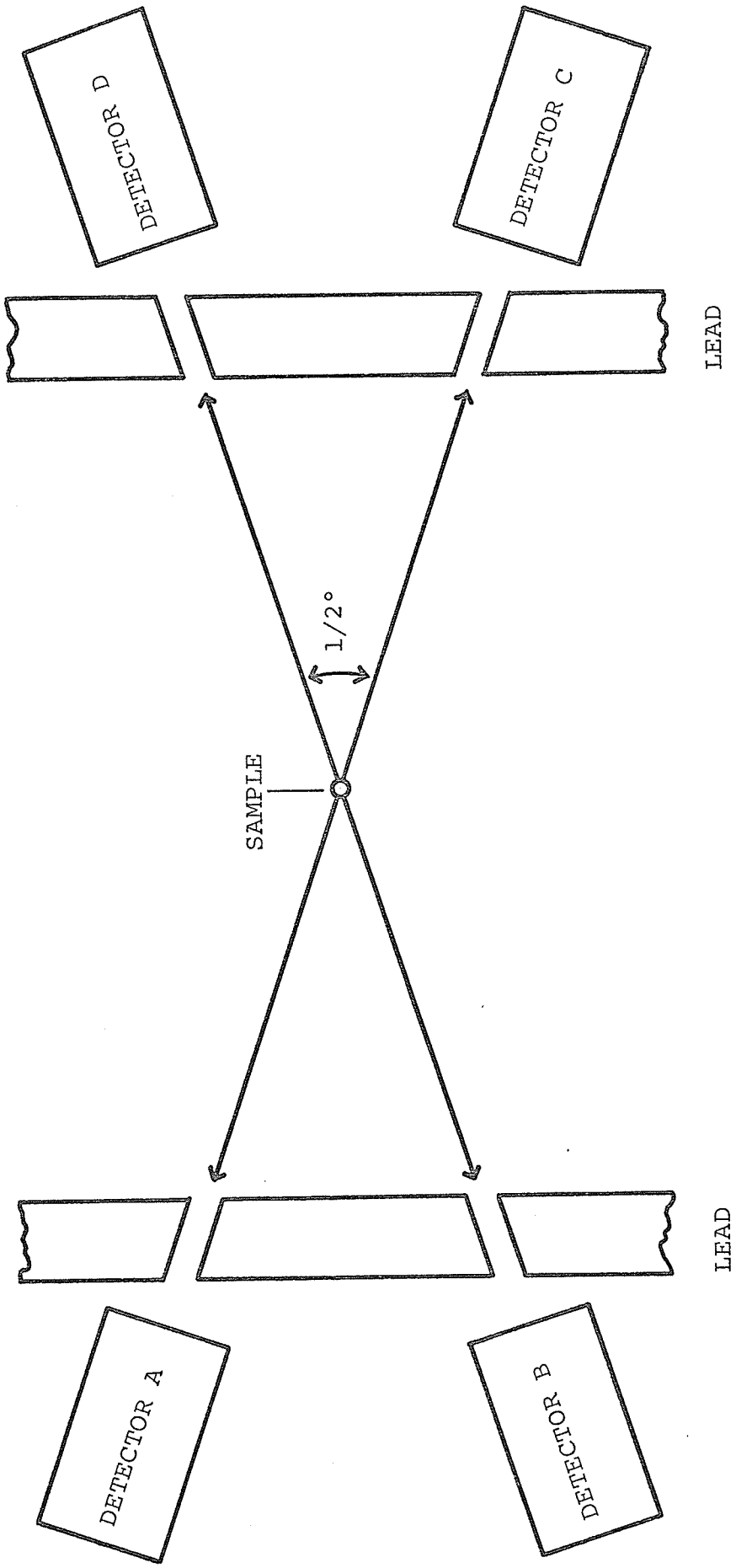

Figure 5. Schematic representation of angular correlation apparatus.

THE DETECTOR ASSEMBLIES

The detectors used were cylindrical NaI(Tl) crystals each optically coupled to its own photomultiplier. The crystal dimensions were 1-in-diam x 2-in . The photomultipliers used were RCA 6342A tubes, operated at 1600 volts.

The two detector assemblies shown in Plates 1 and 2 were located at opposite ends of the apparatus and were identical. Each consisted of four detectors mounted behind an 8-in x 8-in x $2\frac{1}{2}$-in babbit block ($2\frac{1}{2}$-in stops 99% of the 0.511 MeV gamma rays). Four 1/8-in-diam collimating holes were drilled at the corners of a 2.62-in x 2.62-in square inscribed on the face of the babbit block at an angle of 2/3 of a degree from a perpendicular at the center of the inscribed square (see Figure 6). This would ensure that a detector in one detector assembly would align with the detector at the opposite corner of the inscribed square in the other detector assembly.

The detectors themselves were enclosed in 2.62-in-diam brass pipes which were soldered to an 8-in x 8-in x 3/4-in brass plate which was placed directly behind the babbit block. In order to reduce unnecessary gamma ray absorption, 1/2-in-diam holes were drilled in the brass plate which matched the 1/8-in-diam collimating holes in the babbit block. These holes were taped to make them light tight.

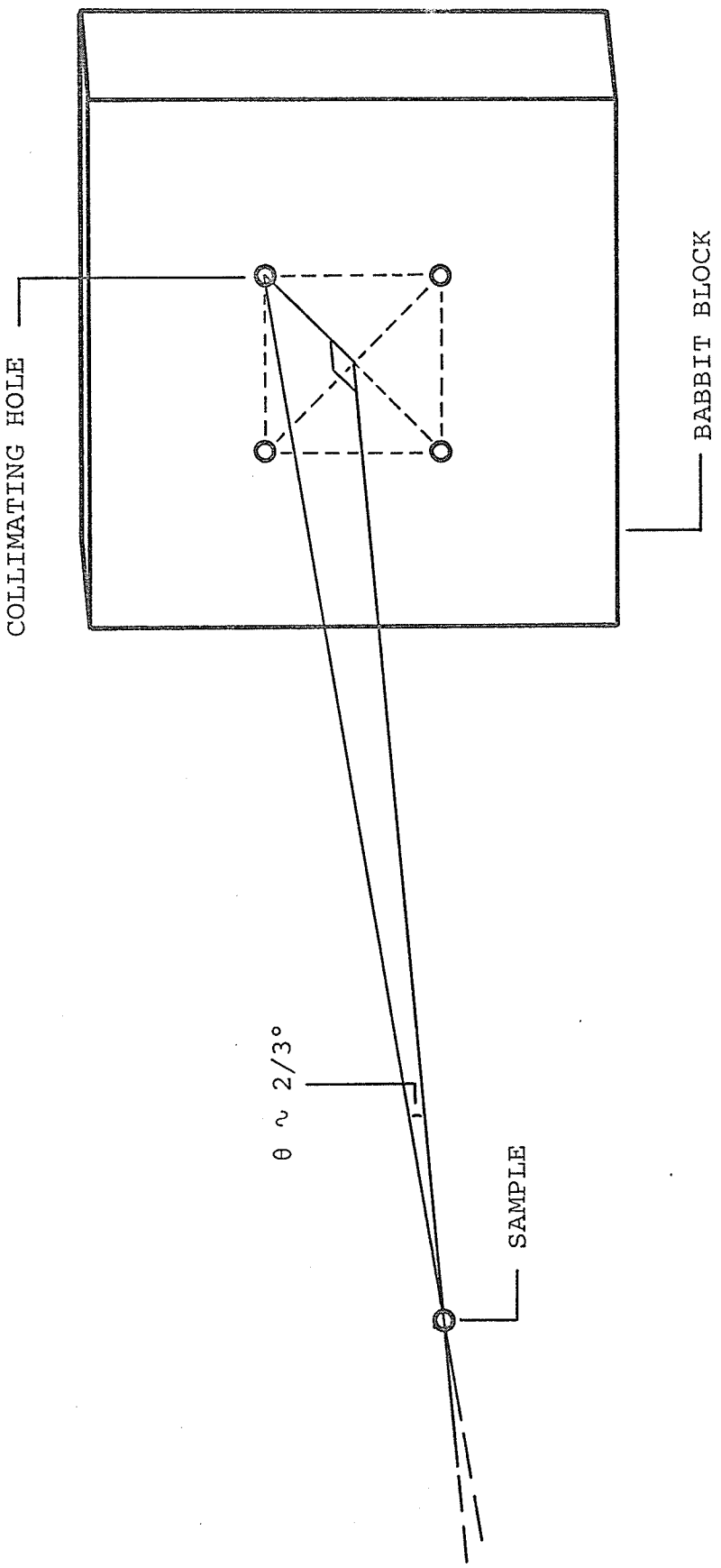

Figure 6. Point detector lead collimator.

Each NaI(Tl) crystal was optically coupled by means of Dow Corning 20-057 coupling fluid to a photomultiplier tube and then securely taped in place. Each tube socket was firmly attached to a brass cap equipped with BNC connectors† for the output signal and the high voltage to be applied to the tube. The brass caps were screwed into the brass pipes making a light tight seal. Before the detectors were placed in the brass pipes, lead shielding collars were placed over each crystal and each photomultiplier tube was enclosed in a co-netic* alloy shield which magnetically shielded all the detectors. The brass plate which supported the detectors and the babbit block were set into another brass plate which served as a base plate for the detector assembly.

One detector assembly was movable (Plate 1) and the other was fixed (Plate 2). The movable detector assembly was mounted on an 8-in x 16-in x 3/4-in steel plate which was free to rotate on top of another similar plate. The two faces which rotated about each other were milled and polished flat and four ball races were set in wells at the corners of the upper plate to allow for easy rotation. A central pivot kept the plates aligned. The bottom plate rode on 24-in long linear rails and was moved by a 3/4-in-diam worm screw, having ten turns per inch, driven by a

---

† Amphenol Canada Ltd.
44 Metropolitan Rd.
Scarborough, Ont.

* R.C.A. Victor Co.,
1001 Lenois St.
Montreal, P.Q.

Plate 1

The movable detector assembly.

Plate 2

The fixed detector assembly.

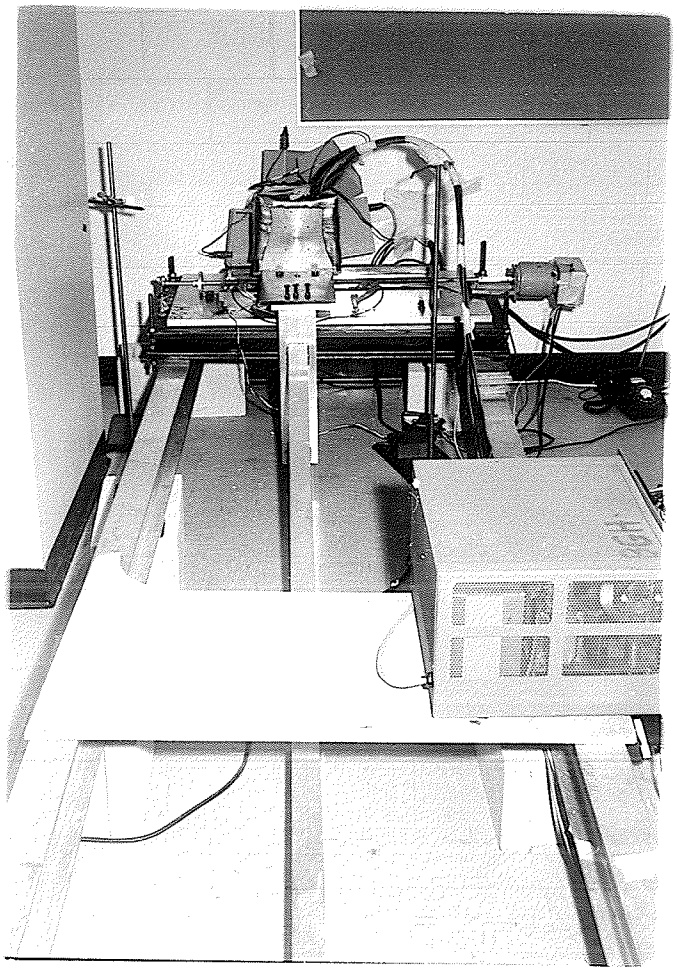

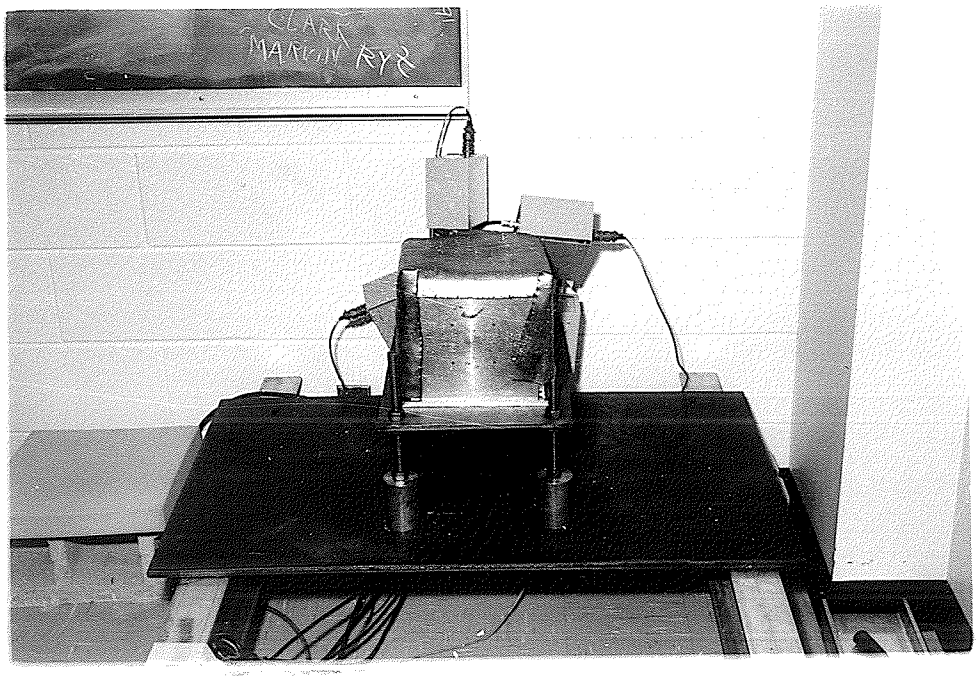

"Slo-syn " reversible motor.† The rails were fixed to a 20-in x 36-in x 3/4-in steel plate which pivoted about a 24-in x 40-in x 3/4-in steel plate in the same manner as the two previously described plates. The bottom plate was positioned above a base plate which was firmly attached to the I-beams. The bottom plate could be adjusted vertically through several inches by turning several nuts positioned on 1/2-in-diam threaded rods which held the bottom plate above the base plate. The detector assembly could be adjusted horizontally by adjusting the screws which held it fixed to the uppermost rotating plate.

The movable detector (Plate 1) was fixed to a 130-in pivot arm of 3-in x 3-in aluminum connected to the uppermost rotating plate. The pivot arm pivoted about the center of the apparatus at a point directly beneath the magnet support. The double pivot at the detectors allowed the detectors to face the sample at all times at a fixed distance from the center of the apparatus as the detectors were moved along the linear rails.

The fixed detector assembly (Plate 2) was mounted on a platform at the opposite end of the apparatus and was adjustable vertically and horizontally in a manner similar to the movable detector assembly. Both detector assemblies were covered with several layers of lead sheet to reduce the background from scattered gamma rays.

---

† Superior Electric Co.
Bristol, Conn., U. S. A.

SOURCE AND SAMPLE ARRANGEMENT

The source and sample were housed in a vacuum chamber of dimension 8-in x 8-in x $3\frac{1}{2}$-in which was located between the pole faces of a fairly large electromagnet (Plate 3). A view of the apparatus within the vacuum box is shown in Figure 7. The vacuum eliminated complications due to annihilation with atmospheric air which could result in distortions in the measured curves.

In order to attain a reasonable coincidence counting rate, it was necessary to adopt a special source and sample arrangement. The positron source was comprised of two copper foils that were irradiated in the Pinawa (WNRE) reactor for periods of time which varied from 16 to 65 hours. The irradiation produced positron active ^{64}Cu with a positron activity of about 300 mC after a 24 hr irradiation. The foils were 2-in x 3/8-in x .002-in strips which were placed in slots in the source holder by hot cell technicians. The source holder, when positioned in the vacuum chamber, held the foils as indicated schematically in Figure 8. The positrons were then magnetically focussed from two sides onto an oriented metal single crystal which was positioned between the copper foils. The source holder formed part of the magnetic circuit resulting in an effective gap of 7/8-in between the pole faces with a measured magnetic field of about 8 kilogauss.

The single crystal samples were tilted through a

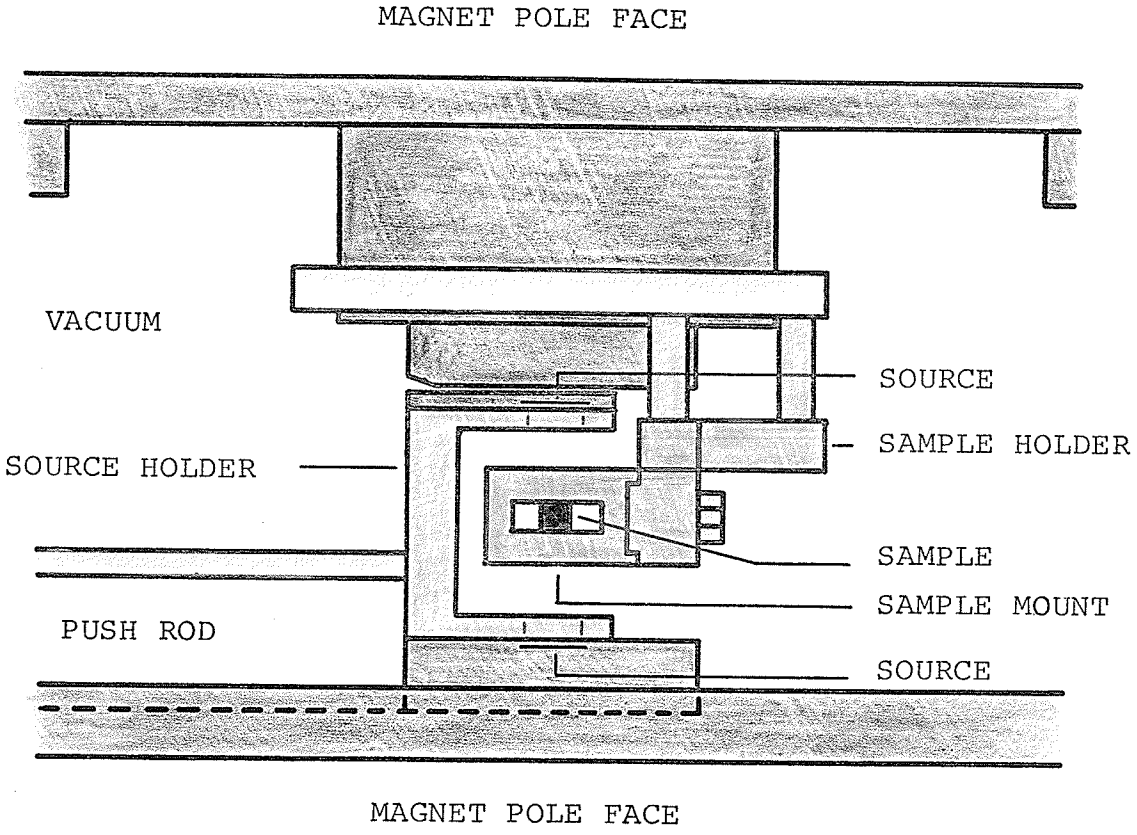

Figure 7. Apparatus within vacuum chamber.

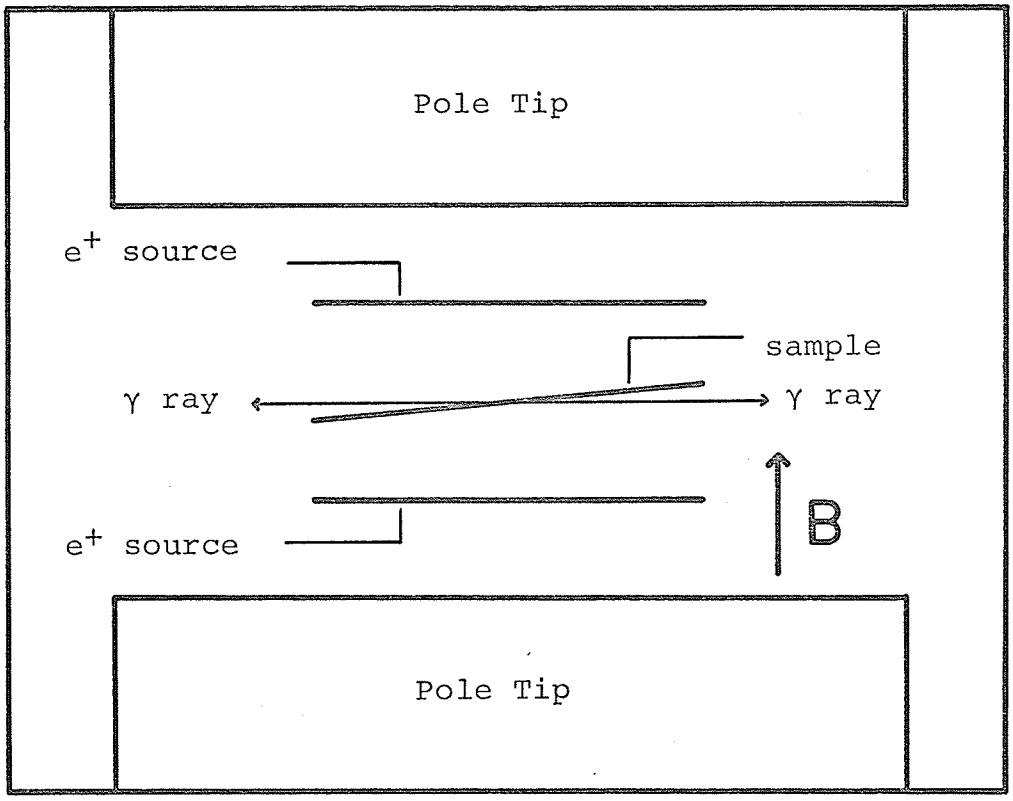

Figure 8. Schematic representation of source and sample arrangement.

Plate 3

The vacuum chamber.

Plate 4

The source holder.

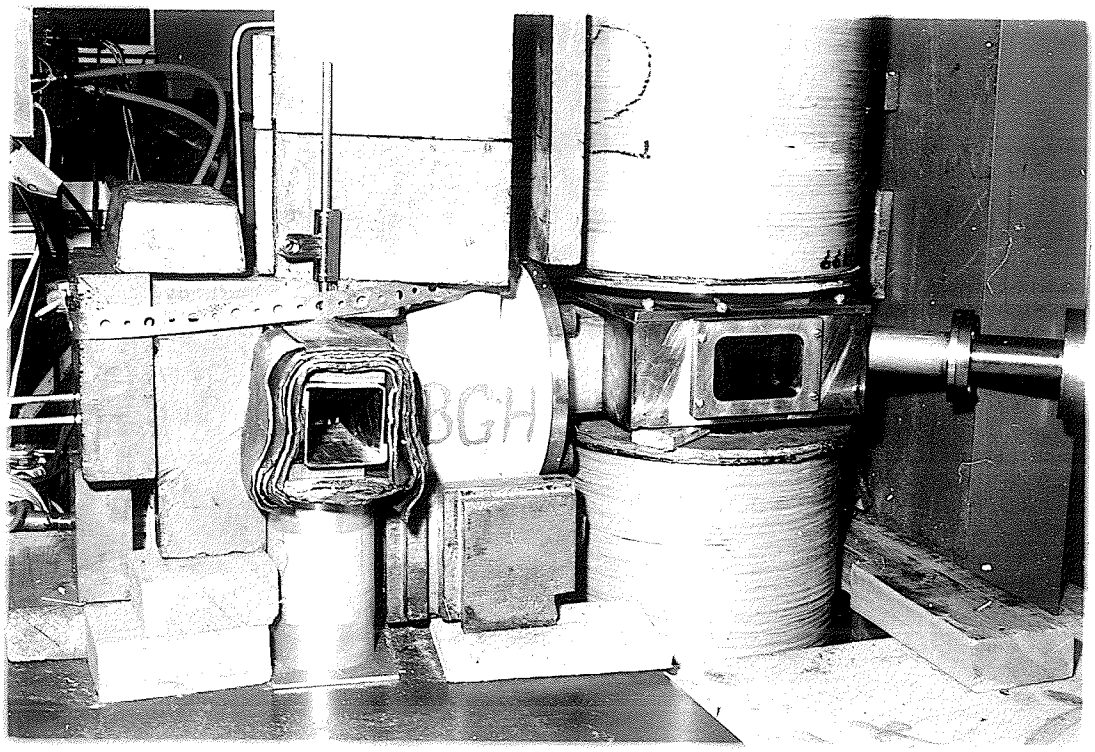

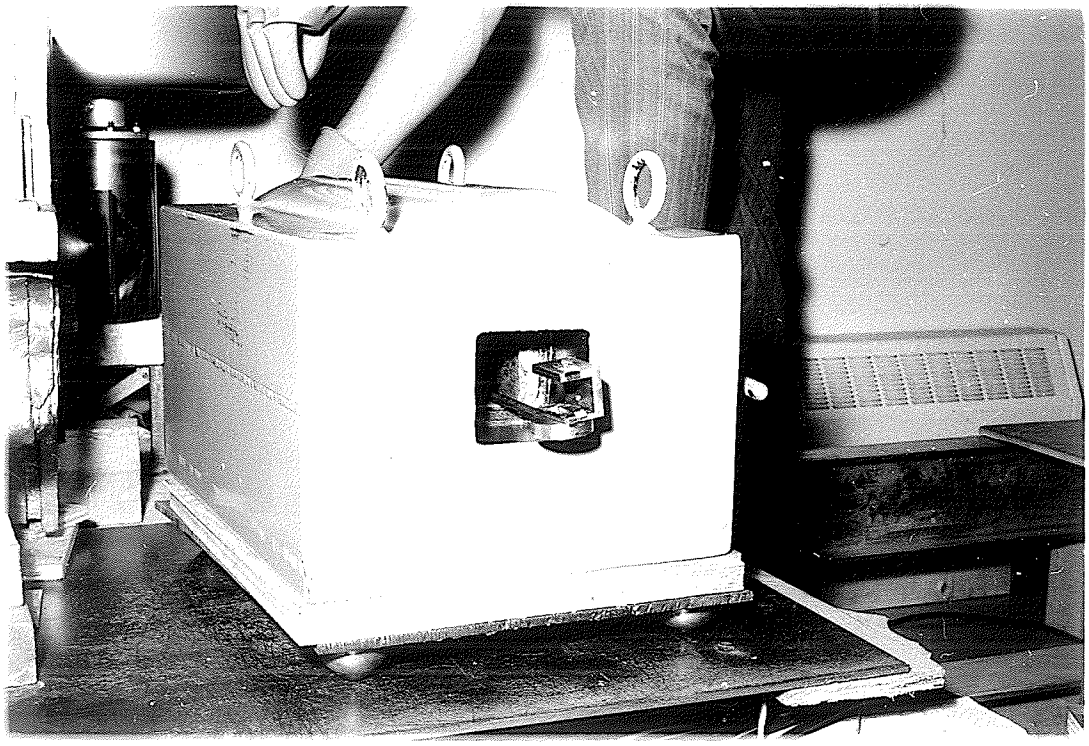

few degrees and made extremely thin in order to minimize the absorption of the gamma rays due to the crystal itself. This reduced the effective thickness of the samples in the direction of the detectors and still provided a relatively large area in which the positrons could annihilate. In addition, the effective area as seen by the detectors was kept relatively small (1/8-in x 1/8-in) to ensure a reasonable angular resolution function.

The sample was collimated at the source to ensure that the source was not seen by the detectors and to reduce the radiation background. Two small lead bricks which were located within the vacuum chamber served this purpose. The gamma rays passed through 3-in x 2-in "kapton" windows† that were 0.001-in thick. The windows were removable to allow for handling of the apparatus within the box.

The source holder (Plate 4) was introduced into the vacuum chamber through an interlock system which allowed the sources to be changed without disturbing the vacuum or the sample (Plate 5). A series of ^{64}Cu sources was necessary to build up the statistics to a suitable level. The sources were handled remotely with the aid of threaded rods which attached to the source holder. The rods were pushed through holes drilled through the lead transfer flask and the lead shielding which surrounded the interlock chamber.

---

† E. I. Dupont Denemours and Co.,
Wilmington, Delaware,
19898 U.S.A.

Plate 5

Source transfer.

Plate 6

Source and sample housing.

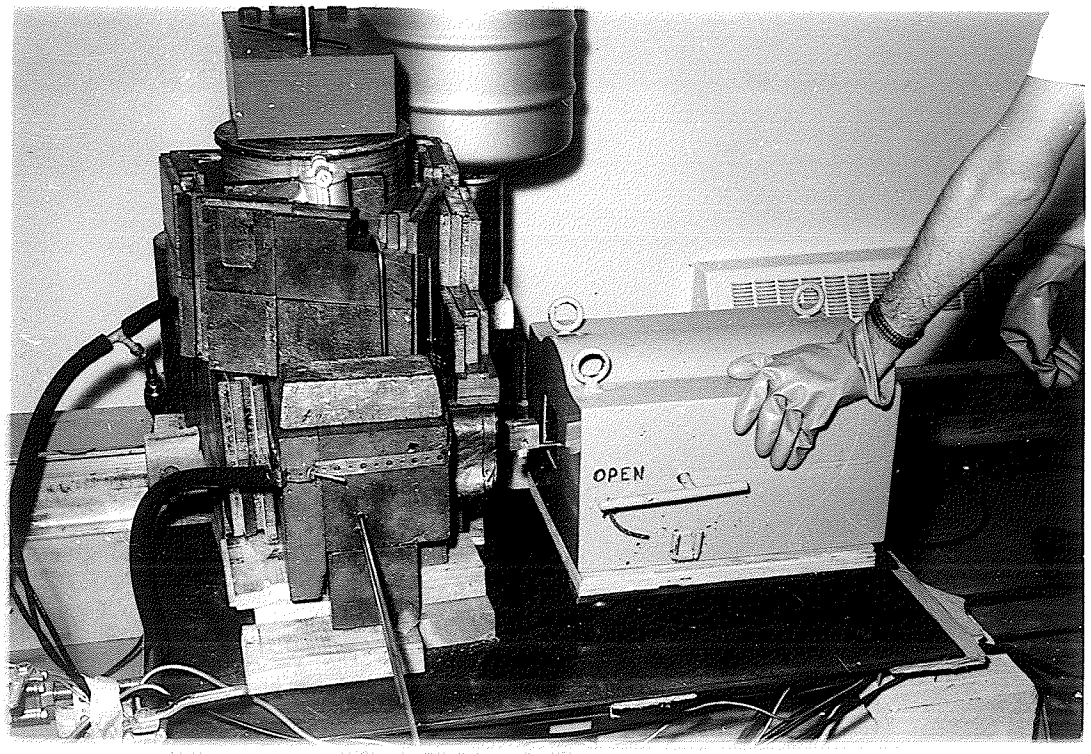
OPEN

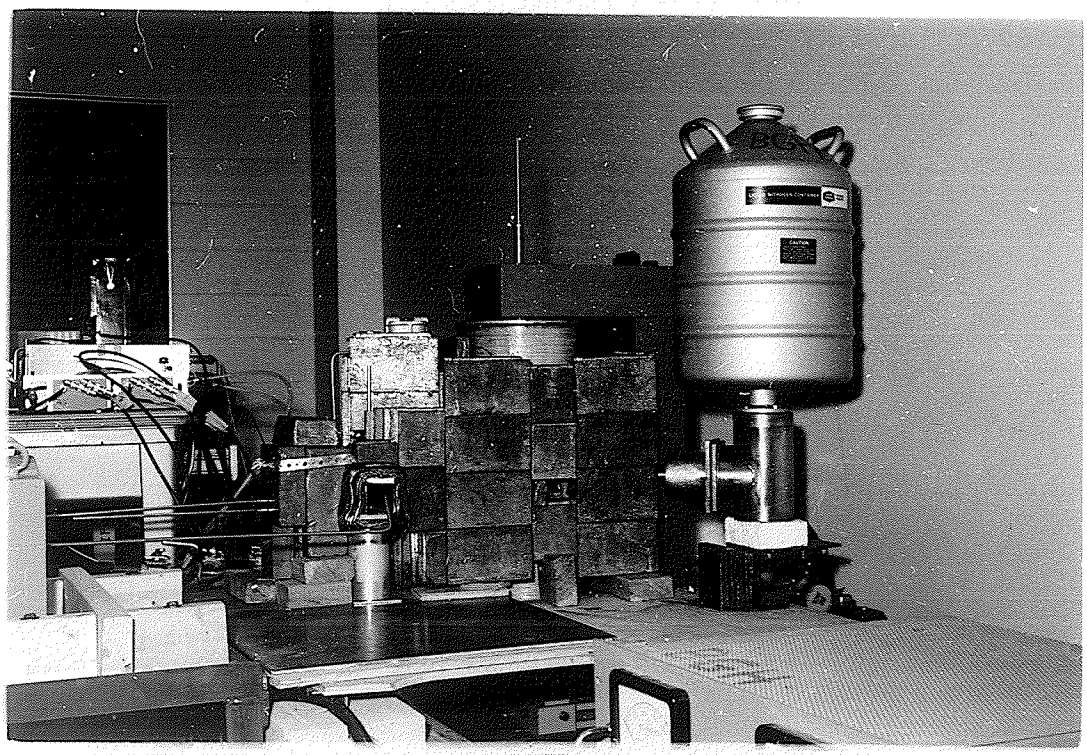

The metal samples were mounted on rectangular copper mounts (see Figure 7) which were designed with openings above and below to allow the positrons to strike the sample and openings at each end to allow the gamma rays to leave the sample. The sample mounts were inserted through the windows of the vacuum chamber and attached to a sample holder which was located permanently within the vacuum chamber. Once the apparatus was aligned with one sample, the sample could be changed without affecting the alignment.

The sample holder was firmly connected to a cold finger and cooling was provided by a 17 liter liquid nitrogen Dewar. A thermocouple was attached to the sample mount and indicated a temperature of about -100°C.

The entire vacuum chamber was surrounded by a wall of 2-in thick lead bricks (Plate 6) which further shielded the positron source. Two openings provided secondary collimation at the source and defined two beams of 0.511 MeV gamma rays that were roughly 2-ft in diameter at the detectors. This was roughly determined by the use of an ordinary Geiger counter.

SAMPLES

All the metal samples were non-oriented single crystals furnished by Metals Research, England. The copper crystal was 99.99% pure. The zinc crystal was 99.999% pure and the magnesium was 99.985% pure. Each crystal was oriented by the back Laué method with an accuracy of about

±2-deg, spark cut into strips and annealed. Various etches were used to thin the samples and to achieve structural perfection at their surfaces. Finally, the condition of each surface was checked by x raying the samples and looking for the Laué spots. The crystal samples were mounted by attaching ordinary copper foil strips to the ends of the crystal samples with Eastman-Kodak 910 contact adhesive (one at each end of each sample). These strips were then attached with the same adhesive to the sample mount.

The copper single crystal sample was spark cut from a 25-mm-diam x 35-mm single crystal and had the dimensions 1/8-in x 1-in x .020-in . The sample was mounted in the sample mount at an angle of 6-deg from horizontal such that the detectors viewed an 1/8-in x 1/8-in effective sample area. The angular correlation curves were measured for the $[1\bar{1}0]$ direction along the direction of the detector motion and the [111] direction in the direction of the measured gamma rays.

The zinc sample was spark cut from a 13-mm-diam x 135-mm single crystal and its dimensions were 1/8-in x 2-in x .020-in . In this case, the crystal was at angle of about 3-deg and the detector motion was along the [0001] direction and the gamma rays were along the $[\bar{2}110]$ direction.

The magnesium sample was also spark cut from a 12-mm-diam x 50-mm single crystal and had the same dimensions as the zinc crystal. The detector motion was in the $[\bar{1}100]$

direction while the gamma rays were along the [11$\bar{2}$4] direction.

ALIGNMENT

The detectors were roughly aligned with the sample and a nominal zero position, corresponding to 180-deg annihilations, was determined by stretching a monofilm fish line through the open windows of the vacuum box which housed the sample. A precision alignment was then performed with an alignment telescope†. The procedure was as follows: Since the apparatus completely filled the room in which it was located, the alignment telescope had to be positioned to one side of the apparatus at a point somewhere between the movable detectors and the vacuum chamber. The movable detector assembly was positioned at the nominal zero position. A 1/8-in-diam pointed rod was inserted into one of the four 1/8-in-diam collimating holes. A needle on a separate stand was then placed in a horizontal position in such a manner that the tip of the needle indicated the position of the pointed tip of the rod which extended slightly out of the collimating hole in the babbit block. The detector assembly was then carefully moved to one side by the motor without disturbing the position of the needle. The telescope was then focused on the image of the needle

---

† Ernst Leitz GMBH Wetzlar Germany

tip in a mirror which was placed behind the needle in such a way that the telescope could also focus on the sample at the center of the apparatus. By careful adjustment of the mirror and the telescope, it was possible to define a straight line which passed through the needle tip and the center of the sample. The fixed detector assembly was then brought into alignment by adjusting the platform on which it stood until the tip of a pointed rod which was placed in the diagonally opposite collimating hole was on the line defined by the telescope. This procedure was applied to two sets of collimating holes to determine what was essentially the vertical alignment of the apparatus. The horizontal alignment was approximate since it was essentially determined by the fish line. The actual zero position of the movable detectors was determined from the experimental data and was found to be slightly different for different samples. This corresponded to slight variations in the horizontal position of the samples when they were mounted in the sample mount. The zero position determined in this way was checked with the alignment telescope and was found to agree within the accuracy of the measurement. It was estimated that the detectors and the sample were aligned with an accuracy of better than .030-in over a distance of 140-in . This corresponds to a value of k_z of about 4% of the Fermi surface radius for copper.

In addition, it was necessary to ensure that the

front face of each babbit block which contained the collimating holes looked directly along the axis of the apparatus. It was estimated that the front faces of both detectors were within 1/2-deg of being perpendicular to the axis. This was not significant in the alignment but was necessary from the point of view of experimental resolution where it would have a significant effect.

THE ELECTRONICS

Four high voltage power supplies provided the high voltage for the eight photomultiplier tubes. They were two NJE corporation model number S-325 power supplies, one Fluke model number 408A power supply and one Fluke model number 413A/AG power supply. Two photomultiplier tubes were connected to each power supply. A block diagram of the detector electronics is shown in Figure 9 for one set of detectors.

The other detectors were identically arranged and fed into the same scaler. The nominal coincidence resolving time of each circuit was 30 nanoseconds. Each photomultiplier was connected to its own preamplifier with a discrimination level set at a threshold of about 140 keV. This circuit produced timing pulses by firing on the leading edge of the photomultiplier pulse. The circuit diagram is shown in Figure 10. Each set of appropriately paired preamplifiers was connected to its own coincidence circuit

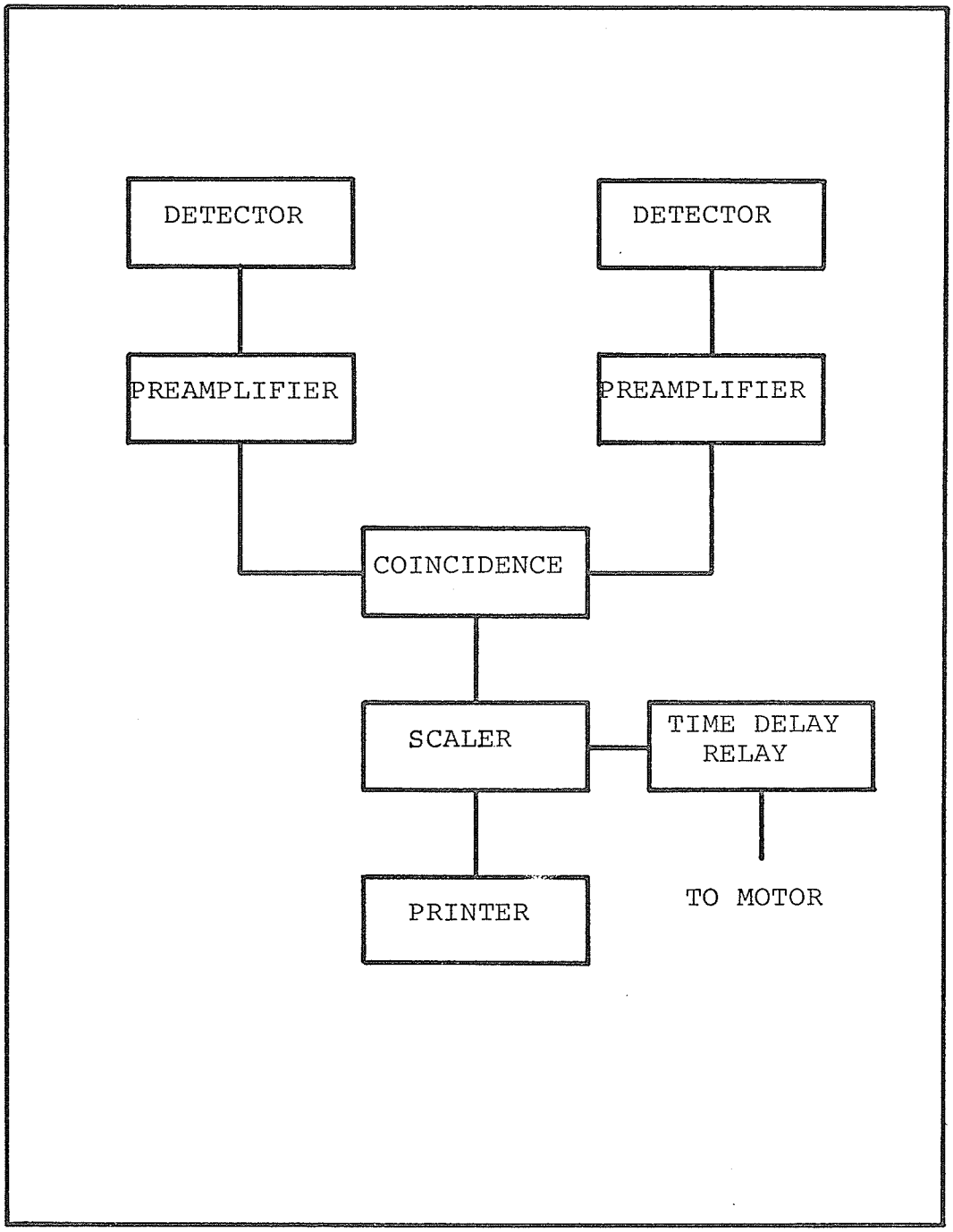

Figure 9. Block diagram of the detector electronics.

which fired on the overlap of the timing pulses. This circuit is shown in Figure 11. The output of each coincidence circuit was then put through a routing circuit (Figure 12) which shaped and channeled the four coincidence signals into a blind scaler (Figure 13). The power for the coincidence circuits was supplied by a Kepco model number ABC 30-0.3 power supply. A Sola constant voltage transformer (catalog No. 30808) was used to maintain the stability of the preamplifier power supplies. The electronics remained quite stable during the course of an experiment.

AUTOMATION OF THE APPARATUS

The whole apparatus was made fully automatic. When the number of counts reached a preset value, a pulse from the scaler activated a time delay relay circuit (Figure 14) which turned on the motor. This motor caused the movable detectors to move to their next position along the linear rails. The printer (a Simplex Timer Recorder) was activated at the beginning and end of each preset count cycle. While the motor was on, the scaler was reset to zero and kept dead until the motor turned off and the printer fired to begin the next cycle.

The position of the detectors was determined by a notched disc which was fixed to the worm screw which moved the detectors. A microswitch which rode near the rim of the disc kept the motor turned on until it fell into the notch thereby shutting the motor off. The time delay relay could

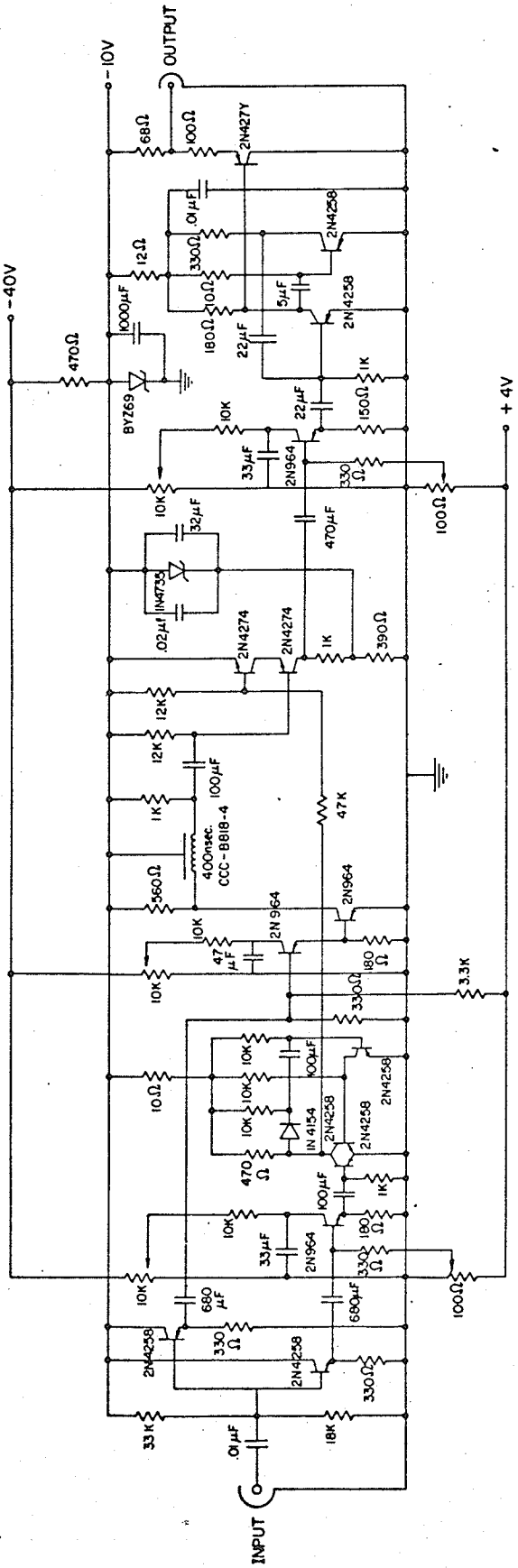

Figure 10. Preamplifier and shaper circuit.

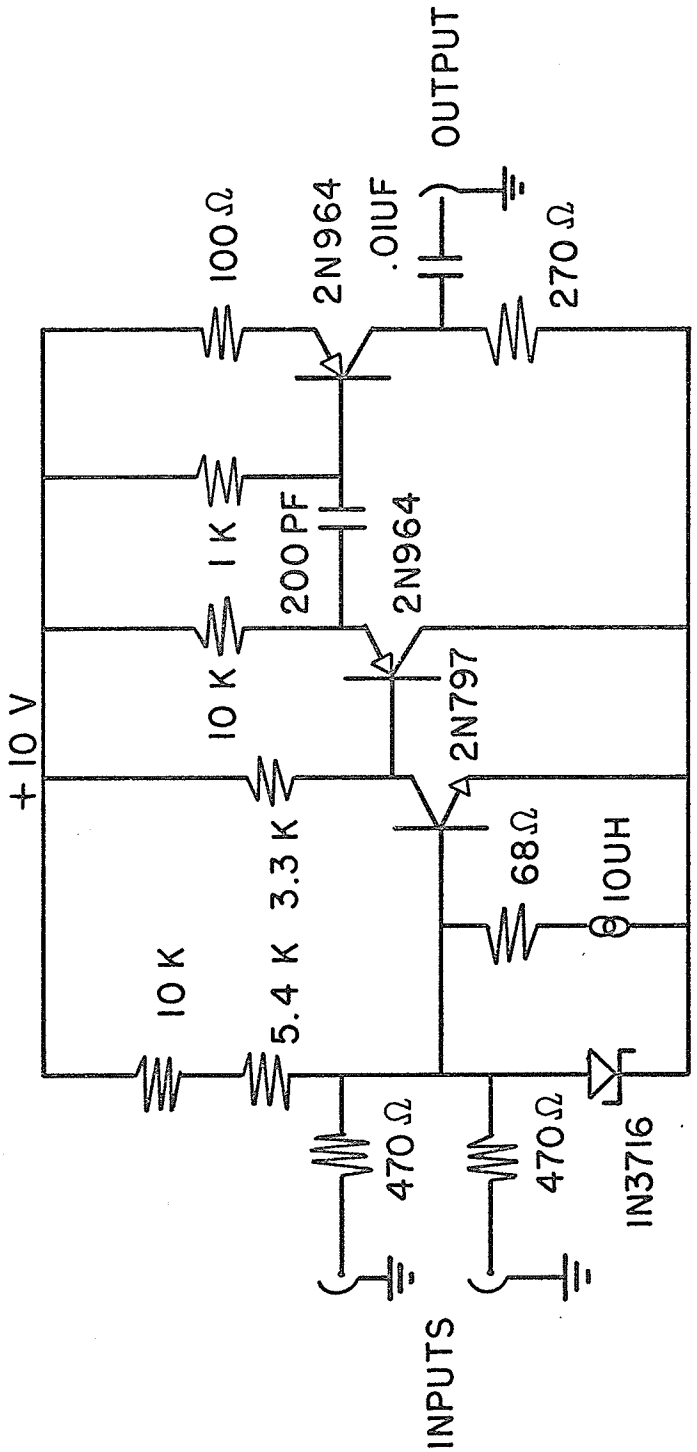

Figure 11. Coincidence circuit.

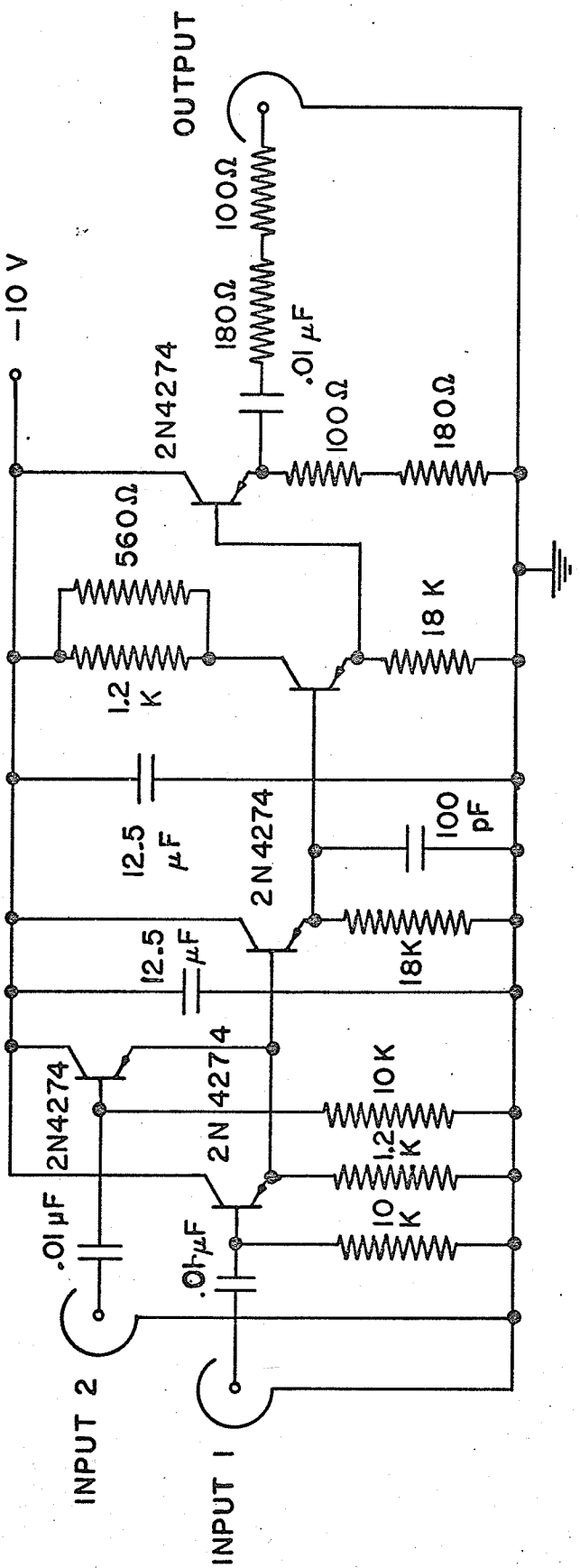

Figure 12. Routing circuit.

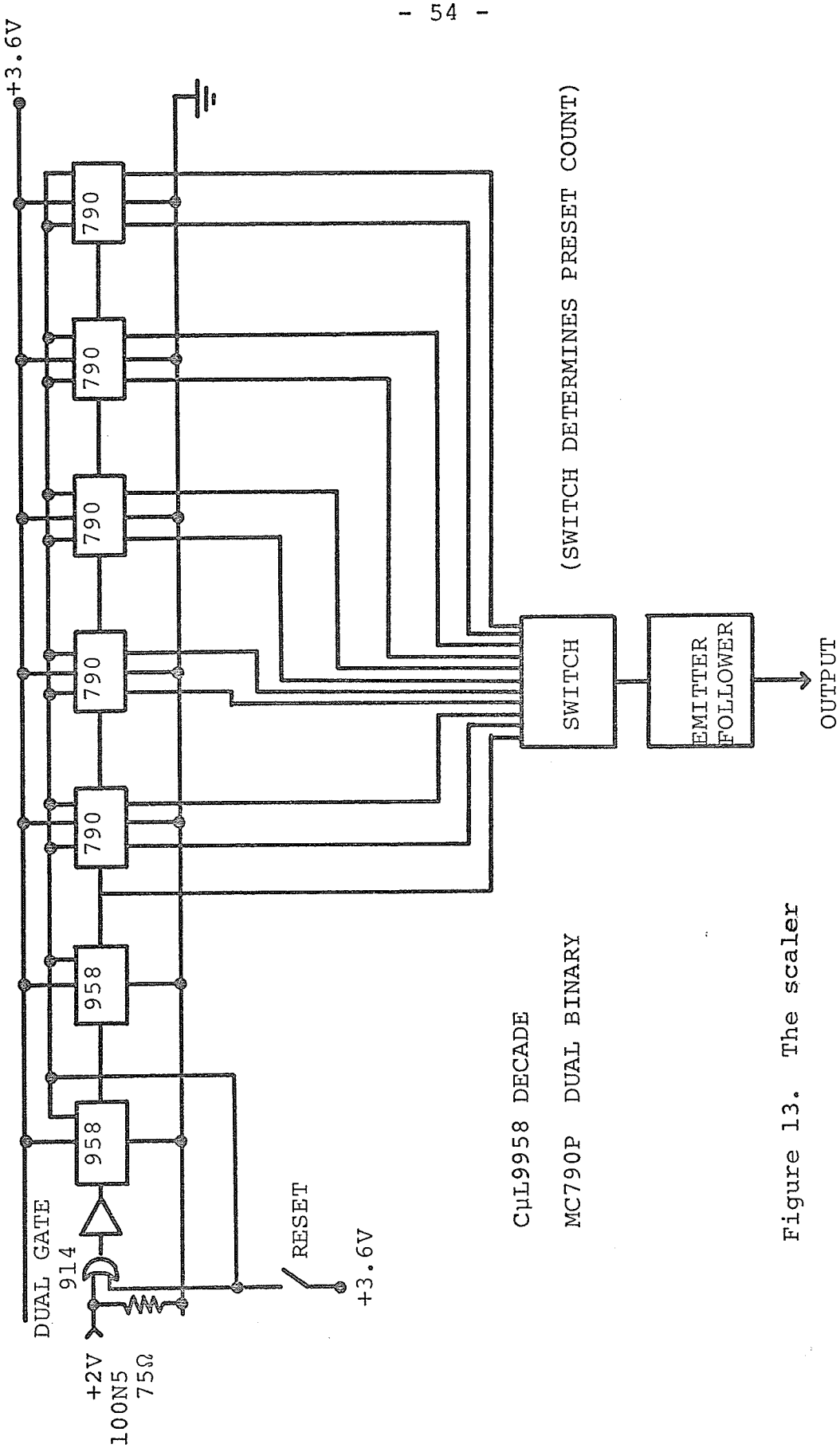

Figure 13. The scaler

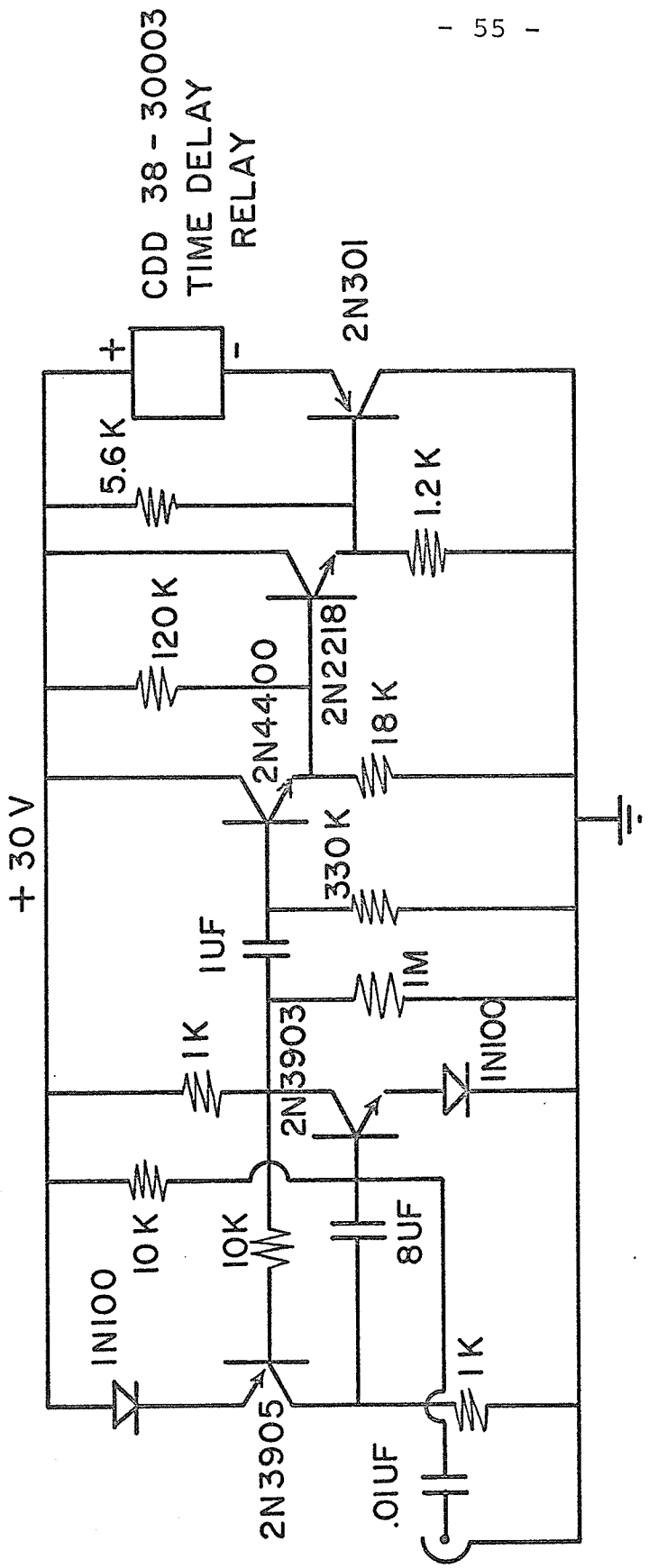

Figure 14. Time delay relay circuit.

be adjusted so that the disc made two revolutions before the motor turned off. This allowed the detectors to move through every second position as determined by the notched disc. One complete revolution of the disc corresponded to 0.684 mrad. The whole range of the angular distribution curve was adjustable by properly spaced reversing microswitches. The data from the printer was in terms of elapsed time and therefore the angular correlation curves were points with constant preset statistics.

THE EXPERIMENTAL PROCEDURE

Each sample was carefully cooled to -100-deg C and kept at approximately this temperature throughout a series of runs which determined the angular correlation curve for the particular sample under study. The sources from the reactor were positioned in the source holder in the hot cells and transferred in a lead castle to the experimental area which was located right at the reactor site. The source was then transferred through the interlock system into place in the vacuum chamber. The magnet was then turned on. The electronics were checked and the singles counting rate was recorded for each detector. The coincidence counting rate was then determined at a position corresponding to the lowest part of the experimental curve as determined by the reversing microswitches. This information determined the setting of the scaler. Data were taken at stops of 100-800

counts at each point of the curve depending on the coincidence counting rate. Counting rates as high 650 counts per minute were obtained at 0-deg. The experiment was started and ran for about two days at which time the source was essentially dead and the counting system was shut off. Several such runs were required to build up the statistics to a reasonable level.

COINCIDENCE RESOLVING TIME

The resolving time of each coincidence curcuit was determined by using the random source method. Two nearly equal sources of gamma rays were placed (one at each end of the apparatus) as close to the photomultiplier tubes and crystals as was possible and the singles rates were measured. The coincidence rates were then measured and the resolving time τ was determined by using the relation

$$N_{ch} = 2\tau N_1 N_2 \qquad (3\text{-}1)$$

where N_{ch} is the chance coincidence counting rate and N_1 and N_2 were the singles counting rates from each of two paired detectors.

The method of adjusting the lengths of the cables between paired detectors and the coincidence box gave a check on the resolving time which was nominally 30 nsec .

THE EXPERIMENTAL RESOLUTION

The experimental resolution was calculated by a computer (Appendix II). The 1/8-in-diam holes which defined the active area of the detectors and the effective area of the sample as seen by the detectors (1/8-in x 1/8-in) were broken up into elements. The grid which corresponded to the movable detector (one detector only) was moved in discrete steps across a grid corresponding to the other detector and the sample. The contributions due to various combinations of the elements were numerically summed for each step to obtain the actual shape of the resolution function. The resulting resolution function was nearly gaussian with a circular cross section and was 1.5 mrad FWHM. In momentum space, this corresponded to the diameter of the cross section of a cylinder through the Fermi surface. The angle ϕ which this cylinder subtends at the origin of the Fermi sphere (see Figure 15) is related to the FWHM value θ_1 = 1.5 mrad by the relation

$$\sin(\phi/2) = m_0 c\theta_1 (2m_0 E_F)^{\frac{1}{2}} \qquad (3\text{-}2)$$

where for copper, for example, the value of ϕ is 13-deg (E_F = 7eV). The [111] necks in the copper Fermi surface subtend an angle of about 20-deg and this feature of the Fermi surface should be within the resolution of the apparatus.

The effect of four sets of detectors did not appreciably worsen the angular resolution of the apparatus. The maximum angle that the four sets of detectors made with

each other was about $1\frac{1}{3}$-deg . This corresponded to four different cylinders in momentum space tilted $1\frac{1}{3}$-deg to each other. This is to be compared with the angle of 13-deg that the intersection of the cylinders at the Fermi surface subtend at the origin.

THE INTERPRETATION OF THE COINCIDENCE COUNTS

The ^{64}Cu positron source had a half-life $\tau_{\frac{1}{2}}$ of 12.7 ± 0.1 hours (Strominger et al, 1958). The errors due to electronic drift and source decay were minimized by recycling the apparatus many times over the preset range in the course of a single run. An adequate number of cycles was obtained by using the following typical preset ranges to obtain the angular correlation curves: θ = -4 mrad to θ = 4 mrad ; θ = 4 mrad to θ = 7 mrad ; θ = 7 mrad to θ = 21 mrad .

The apparatus measured the elapsed time Δt for a preset number of counts N over a preset range of θ. The time independent angular correlation $N(\theta)$, corrected for source decay and chance coincidences, was determined by using the relation

$$N(\theta) = \{N(\Delta t)^{-1} - N' e^{-2\lambda\Delta t}\} e^{\lambda\Delta t} \qquad (3\text{-}3)$$

where $\lambda = 0.693/\tau_{\frac{1}{2}}$ and N' was given by equation (3-1) where N_1 and N_2 were the singles counting rates at the beginning of a run. A computer calculated $N(\theta)$ for the four sets of detectors (Appendix III). The results for each run were

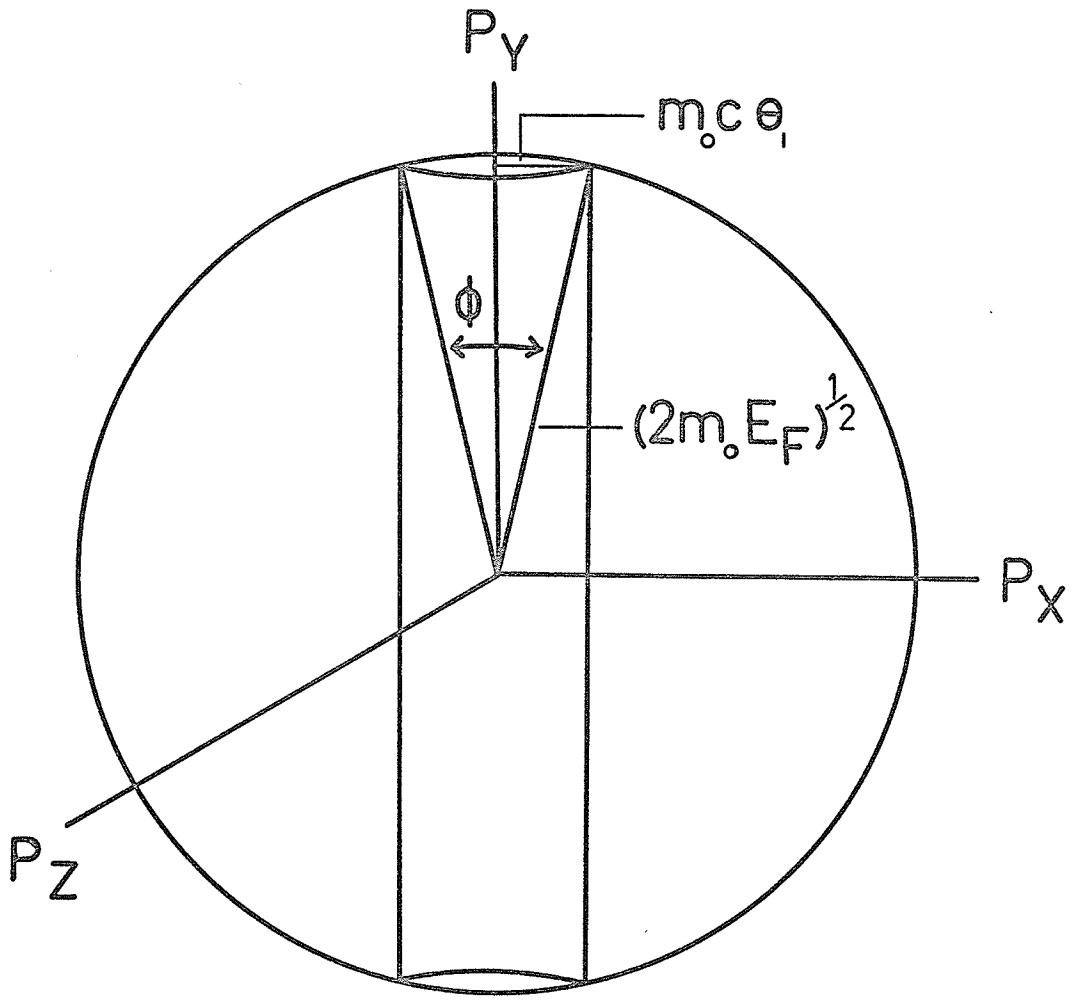

$\phi \sim 13°$ for copper

Figure 15. Experimental resolution.

normalized and then averaged with greater weight being given to runs with better statistics.

In the extreme core region of the experimental curves where the coincidence counting rate was quite low, the chance coincidence counting rate became serious. As the run progressed, however, the chance rate dropped as the square of the elapsed time and the true coincidence rate became a higher percentage of the actual counting rate. The results for the latter passes of the detectors were, therefore, given a greater weighting than the results for the earlier passes.

The timer ran 10% fast and a corresponding correction was made to the computer program. There was also a slight backlash in the worm screw which corresponded to about 0.07 mrad . This systematic error was small compared to the experimental angular resolution and was ignored and the results for passes in opposite directions were simply averaged.

The experimental points were plotted and the center of each curve was determined by folding the plot on a light box and matching the two sides of the curve. The data for $\theta < 0$ were then folded over onto the data for $\theta > 0$ and the agreement of the points provided a check on the experimental technique and the treatment of the data. The statistical errors were indicated on most data points unless the errors were smaller than the experimental points themselves.

The number of counts in the peak was of the order

of 10,000 for copper and zinc and of the order of 35,000 for magnesium. In the core region, the number of counts was about 200-500. Typical maximum coincidence counting rates were about 100 per minute for copper, 200 per minute for zinc and 600 per minute for magnesium. The singles counting rates were typically 20,000 counts per minute for copper, 40,000 counts per minute for zinc and 50,000 counts per minute for magnesium.

CHAPTER 4

RESULTS AND DISCUSSION

The results are shown in Figures 16, 17, 19-25. Single crystal studies of zinc and magnesium have not been performed before using the point slit method. Copper, on the other hand, has been investigated extensively in both the point and crossed slit geometries. The reason that copper has emerged as a test case is of a technical nature. Neutron irradiation of the copper crystal specimen under study produces ^{64}Cu (the positron source) within the sample itself. This containment results in relatively strong positron sources, high counting rates and improved angular resolution over previous methods which have used external sources (Fujiwara and Sueoka, 1966; Williams et al, 1965). The apparatus described in this thesis, however, represents an advance in design of this kind of apparatus and achieves a comparable angular resolution and counting rate without having to subject the crystal specimen to neutron irradiation. The use of an external source also permits the study of materials other than copper and copper alloys.

Experimentally, it has been found that positrons are quite sensitive to defects in crystals (Conners et al, 1970). It is desirable, therefore, to determine the extent to which neutron irradiation may cause crystal damage and the

effect it may have on the shape of the measured momentum distributions for copper single crystals. As a check on the technique of using in situ positron sources, we have measured the angular distribution of the annihilation radiation for an annealed single crystal of copper into which positrons were focussed from an external source.

The results can be seen in Figure 16 which shows a comparison of the data obtained using the annealed copper single crystal with data (sample B) obtained by Becker (1969) at U.B.C. for the same crystal orientation and using a very similar angular resolution. The two sets of data were normalized to each other at the peak. The unannealed copper crystal (sample B) was neutron irradiated for about 48 hours in the AECL reactor at Chalk River and the angular correlations of the annihilation radiation due to the induced ^{64}Cu activity were studied starting approximately 36 hours after the sample was removed from the reactor.

The sample B data drops about 15% below the sample A data at θ=8 mrad which is consistent with the results of Conners et al (1970) where such an effect is attributed to positron annihilation in vacancies. The effect, however, is not very large and the two sets of data have a similar shape.

In general, the results obtained for the three metals studied, copper, zinc and magnesium exhibit the expected features – a distribution peaked at small θ falling off rapidly with angle as θ approaches the Fermi cut off

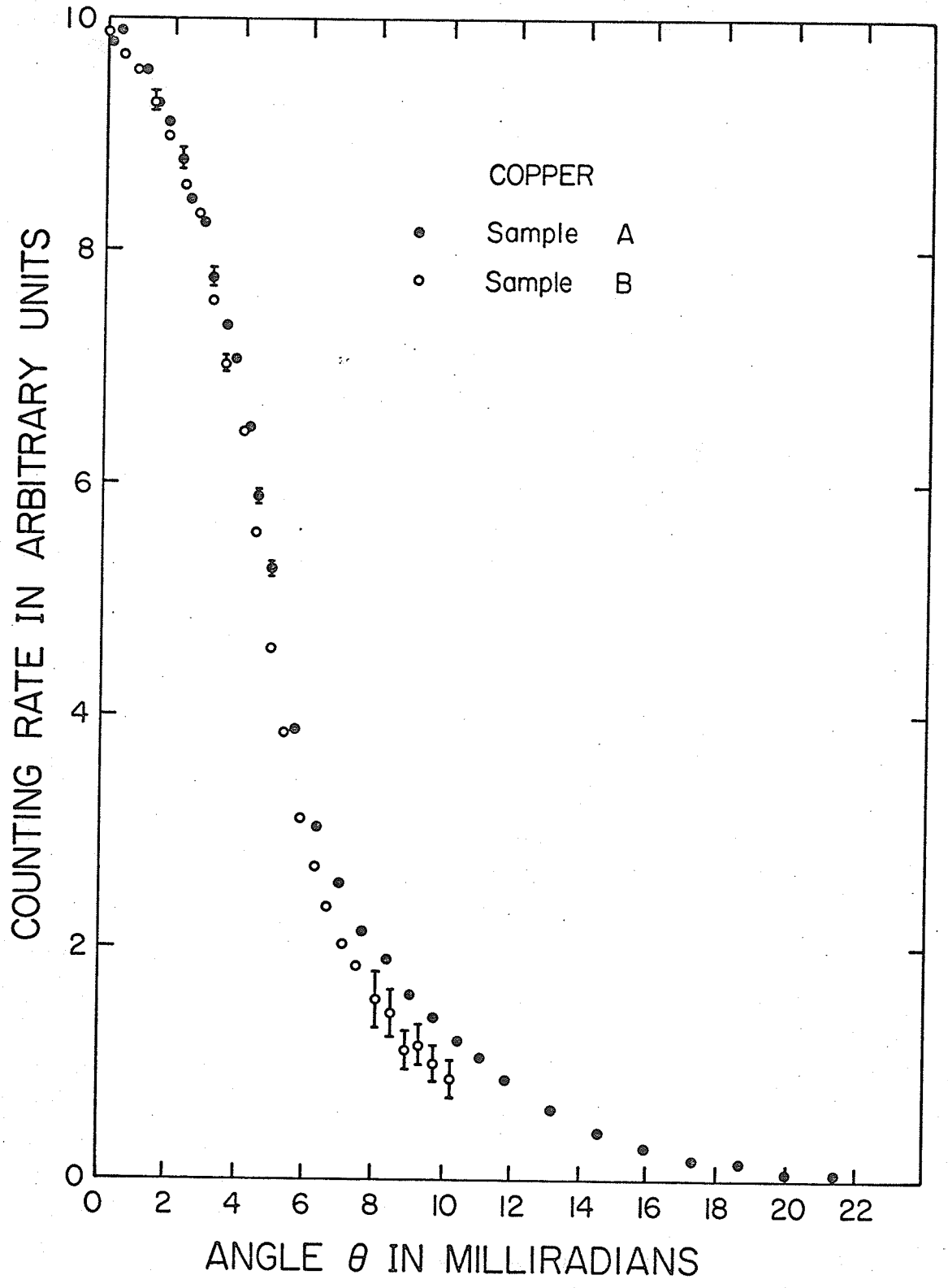

Figure 16. Comparison of an annealed single crystal of Cu — $(1\bar{1}0)$Axis, (111)γ-ray — with a neutron irradiated Cu sample of the same orientation.

value and then tailing off gradually for larger values of θ. The essential difference between the results obtained for each of the metals studied is, as expected, in the size of the observed tail, being greatest in the case of copper and the smallest in the case of magnesium. This is consistent with the assumption (Berko and Plaskett, 1958) that the tail is mainly due to annihilations with core electrons since the core electrons of magnesium are quite tightly bound and so have a small overlap with the positron whereas the 3d electrons of copper can be excited into the conduction band resulting in a greater overlap. Zinc is an intermediate case. The magnesium results attest to the precision of the apparatus since an observed large tail in the magnesium distribution is not to be expected and would imply poor angular resolution.

The experimental data are analyzed by superimposing a calculated conduction electron distribution on a theoretical core distribution which is fitted to the experimental points in the high momentum part of the curve.

The conduction electron distribution is calculated by appropriately weighting Fermi surfaces situated at reciprocal lattice sites and summing the contributions from all the contributing "spheres" in the manner described in Chapter 2. This was accomplished by performing a numerical calculation on a computer (Appendix IV).

Two different types of core distributions have been calculated by Gould (1971) both of which use a tight

binding approximation for the core electrons but each with a different approximation for the positron wavefunction.

The first method (method A) of calculating the core contribution follows the method of Stroud and Ehrenreich (1968) and is described in detail by West et al (1971). The method uses a realistic positron wavefunction (a plane wave expansion over reciprocal lattice vectors) to calculate the electron positron overlap integral. The positron is assumed to see a potential due to a positive ion core computed without exchange together with a potential due to a uniform charge distribution of one or two electrons per atom. The core electron wavefunctions are taken from Herman and Skillman's (1963) atomic structure calculations. The calculation, which takes the symmetry of the crystal into account, has been performed for both fcc and hcp structures.

The second method (method B) of calculation uses a positron wavefunction calculated in the Wigner-Seitz approximation. The positron sees the same potential as is used in method A but the calculation does not invoke the crystal symmetry and results in an isotropic distribution. This method has not been applied earlier to results obtained using the point geometry.

Both of the above methods result in higher momentum components in the positron wavefunction to be used in calculating the corresponding conduction electron distributions. The resulting curves are made up, therefore,

of contributions from various sites in the reciprocal lattice. Calculation shows that in most cases, these contributions are relatively small for the point geometry. They can be important, however, in the long slit geometry (West et al, 1971).

The results obtained for copper are shown in Figures 17 and 18. The core electron annihilation contribution was, in each case, calculated as being due to the 3s, 3p and 3d shells, the inner shells being neglected due to the small electron positron overlap for them. The experimental resolution was folded into the theoretical core electron distribution (Appendix V). The positron wavefunction as calculated by method A included 145 plane waves. The conduction electron contribution was calculated by folding the experimental resolution into a distribution obtained by assuming a spherical Fermi surface having a free electron radius of 5.25 mrad with cylindrical necks extending to the Brillouin zone boundary in the (111) directions (Appendix IV). A sketch of the Fermi surface of copper is shown in Figure 19.

Higher momentum components in the positron wavefunction are shown in Table I together with the higher momentum components previously calculated by Berko and Plaskett (1958) for conduction electrons near $\underline{k}=\underline{0}$. These two sets of components have been combined to obtain the Fourier components for the product wavefunction and these are also shown in Table I along with the product components

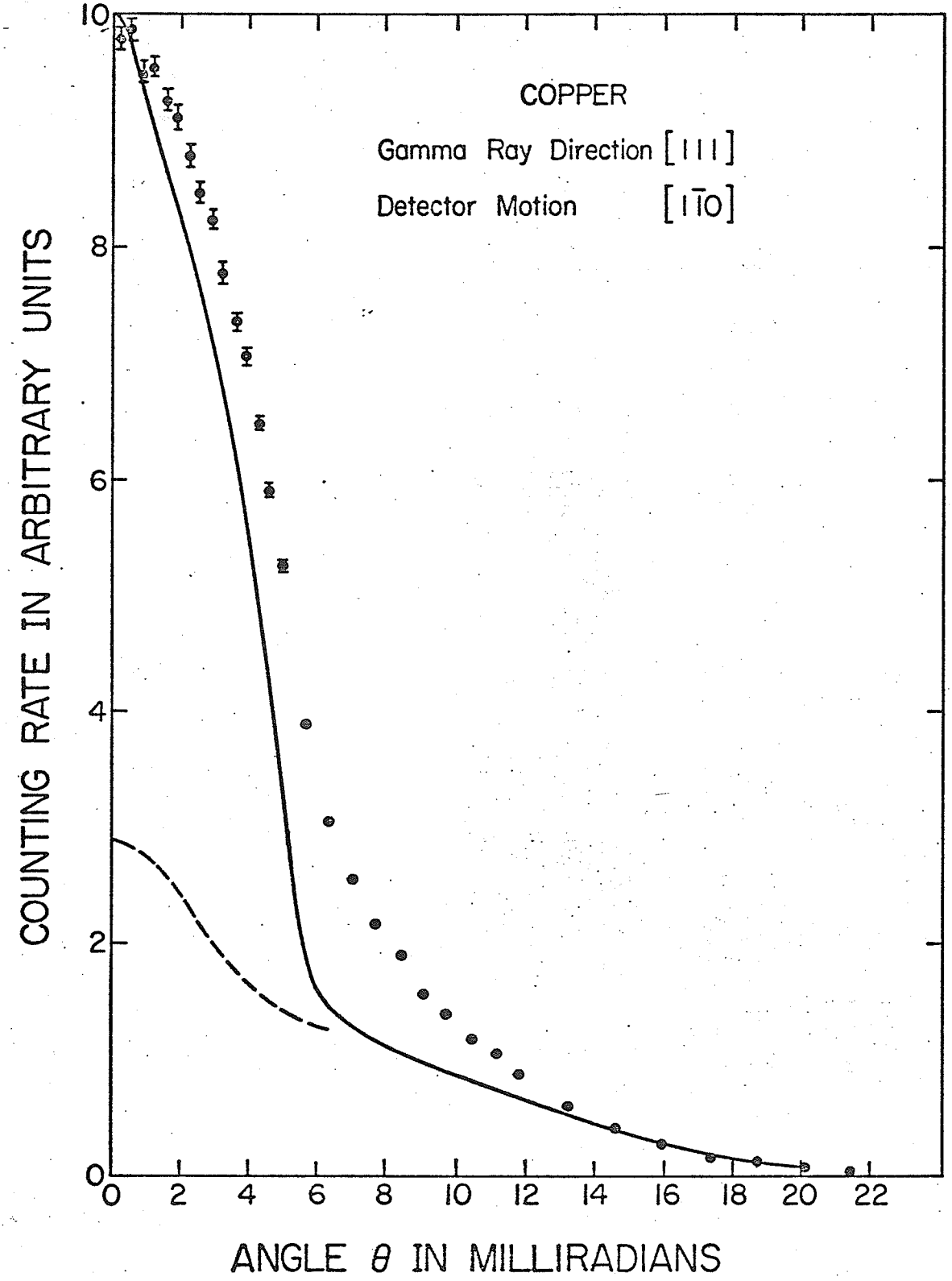

Figure 17. Copper results with theoretical fit as calculated by method A. The dashed line is the calculated core contribution.

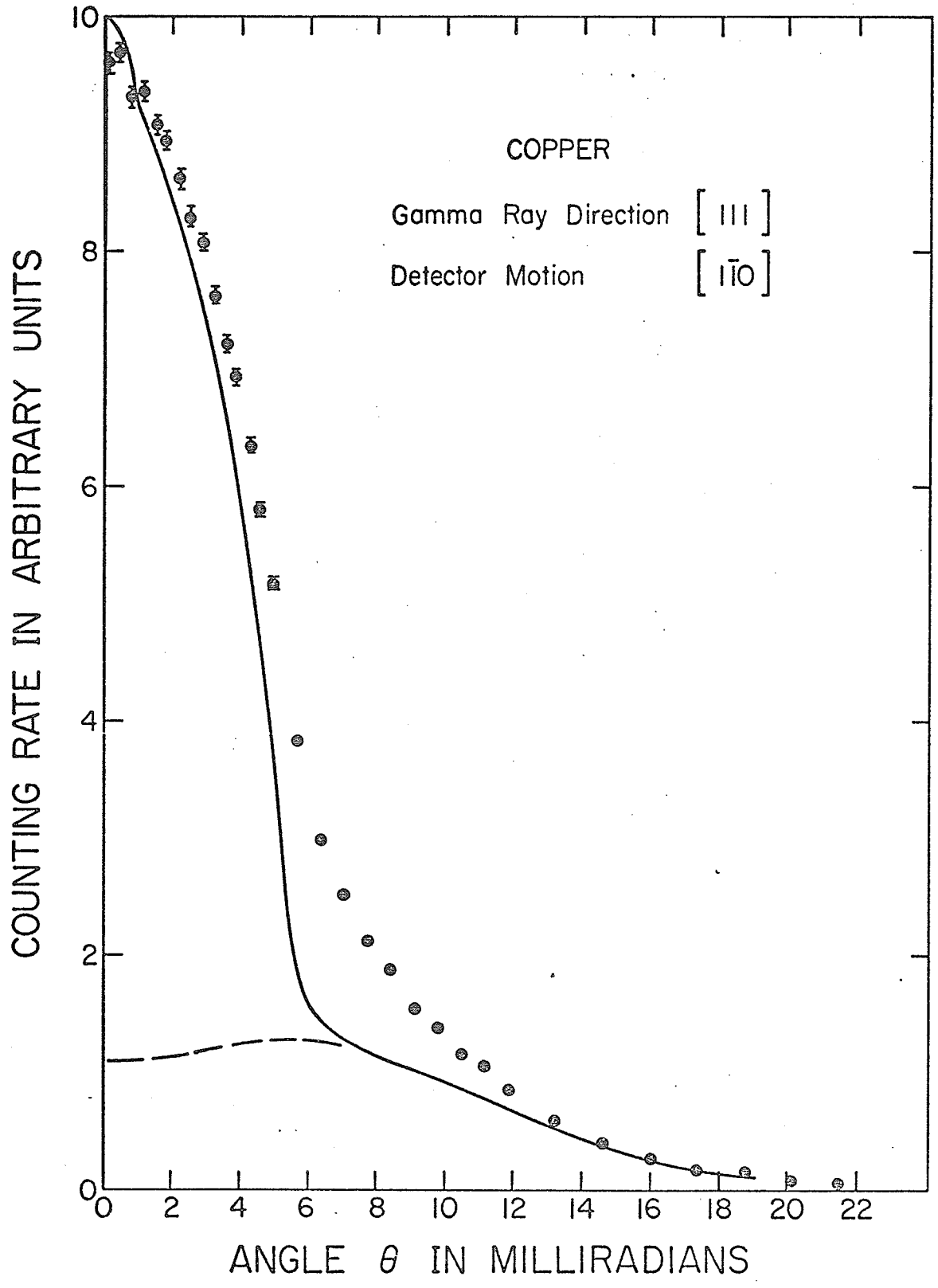

Figure 18. Copper results with theoretical fit as calculated by method B. The dashed line is the calculated core contribution.

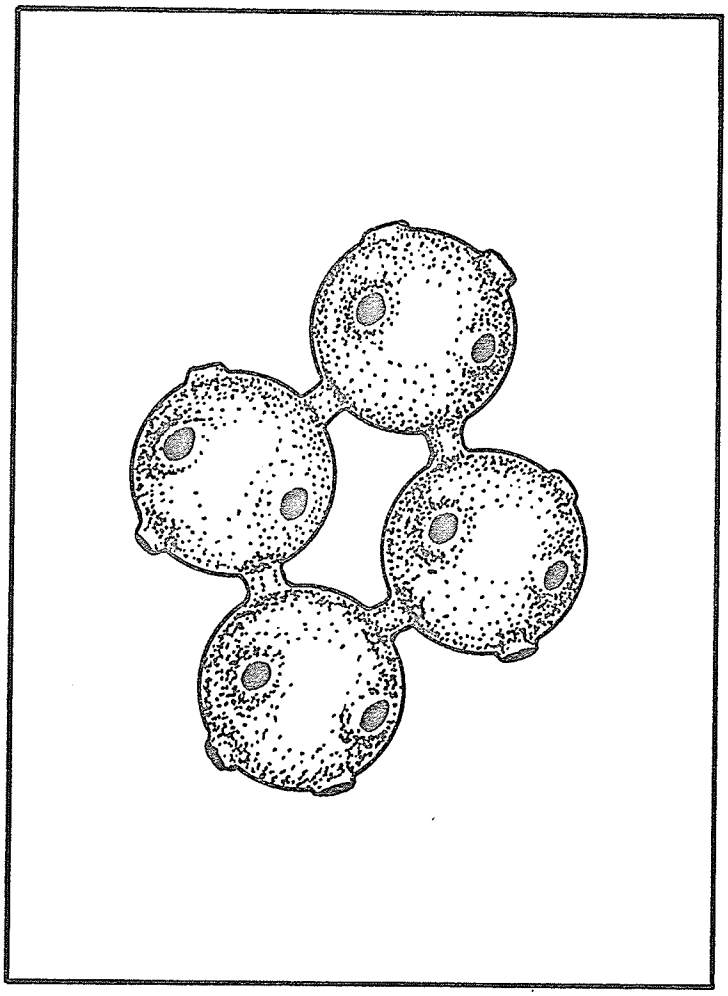

Figure 19. A sketch of the Fermi surface of copper.

Table I. Table of Fourier components for copper. ($a_{\underline{G}}$ are the positron Fourier components. $b_{\underline{G}}$ are the electron Fourier components. Ω is the volume of the unit cell. The superscript BP refers to Berko and Plaskett (1958).)

$\underline{G}$	(000)	(111)	(200)	(220)	(311)
$a_{\underline{G}}$	0.1089	-0.0083	-0.0045	-0.00071	-0.00025
$a_{\underline{G}}^{BP}$	0.1086	-0.0077	-0.0055	-0.0010	-0.0001
$b_{\underline{G}}^{BP}$	0.0983	-0.0140	-0.0110	-0.0041	-0.0019
$\Omega\Sigma_{\underline{G}'} a_{\underline{G}'} b_{\underline{G}-\underline{G}'}^{BP}$	0.955	-0.135	-0.079	-0.007	0.003
$\Omega\Sigma_{\underline{G}'} a_{\underline{G}'}^{BP} b_{\underline{G}-\underline{G}'}^{BP}$	0.953	-0.127	-0.087	-0.009	0.006

previously calculated by Berko and Plaskett (1958). These product components were used in calculating the conduction electron contribution to the angular correlation curves. It is to be noted that the Fourier components for the two different positron wavefunctions (both of which are shown in Table I) are not very different from each other.

Figures 20 and 21 show the results obtained for zinc and Figures 22 and 23 show the results obtained for magnesium. The core electron annihilations were calculated as being due to the M shell of zinc and the L shell of magnesium. The positron wavefunction of method A used 221 plane waves for both zinc and magnesium. The Fermi surfaces of zinc and magnesium were approximated by spheres (Reed and Brennert, 1963 (Zn); Stark, 1967 (Mg)) in the calculation of the conduction electron contribution. The free electron values were used for the radii of these spheres (6.06 mrad for zinc and 5.25 mrad for magnesium). Only the higher momentum components of the positron wavefunction were included and these are shown in Table II. The experimental resolution was folded into both core and conduction electron contributions.

A comparison of the results obtained with the two methods of calculating the core distributions indicates a marked difference between them. In general, the results obtained by method A rise sharply as θ approaches zero while the results obtained by method B are much flatter and, in

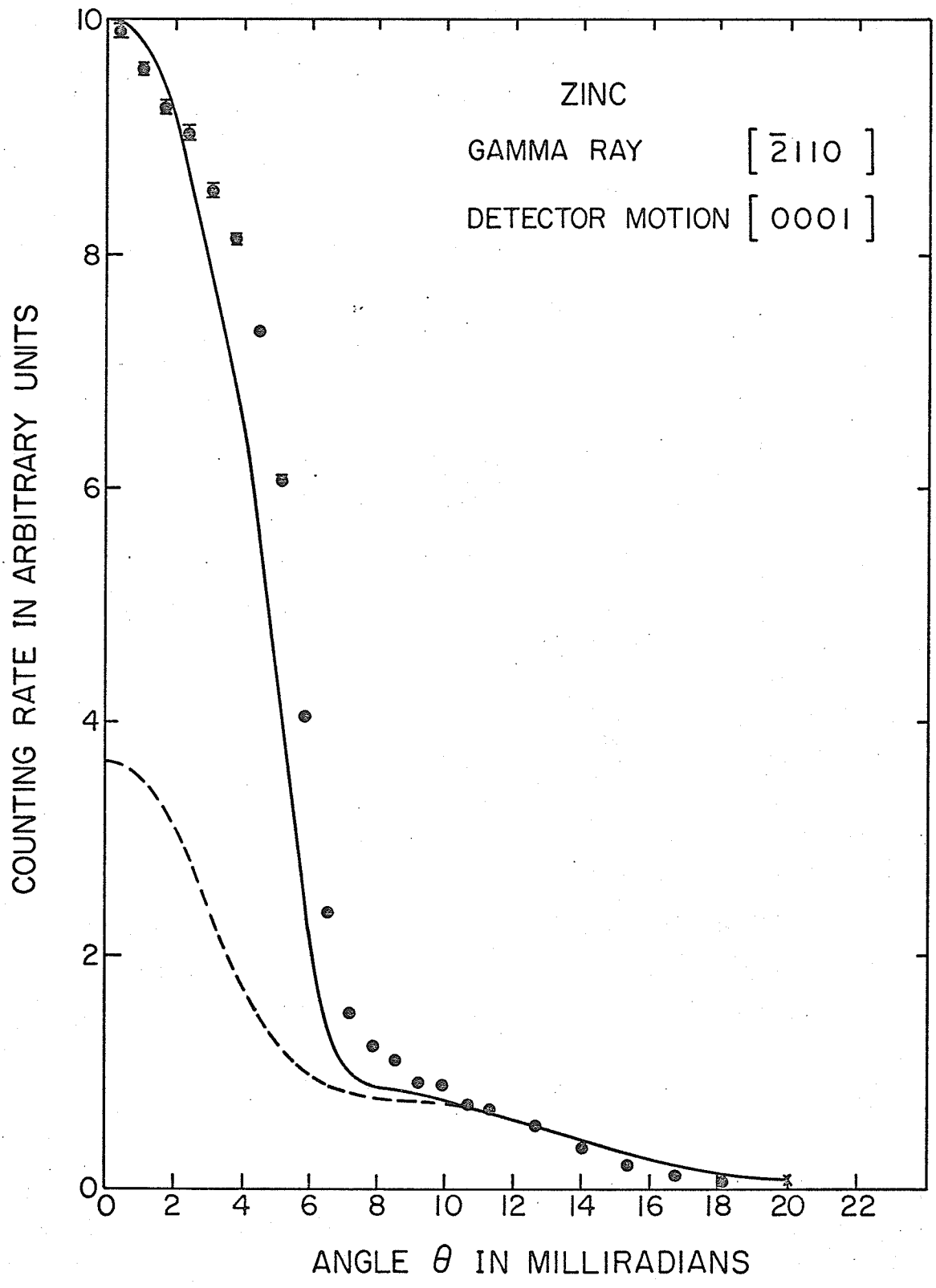

Figure 20. Zinc results with theoretical fit as calculated by method A. The dashed line is the calculated core contribution.

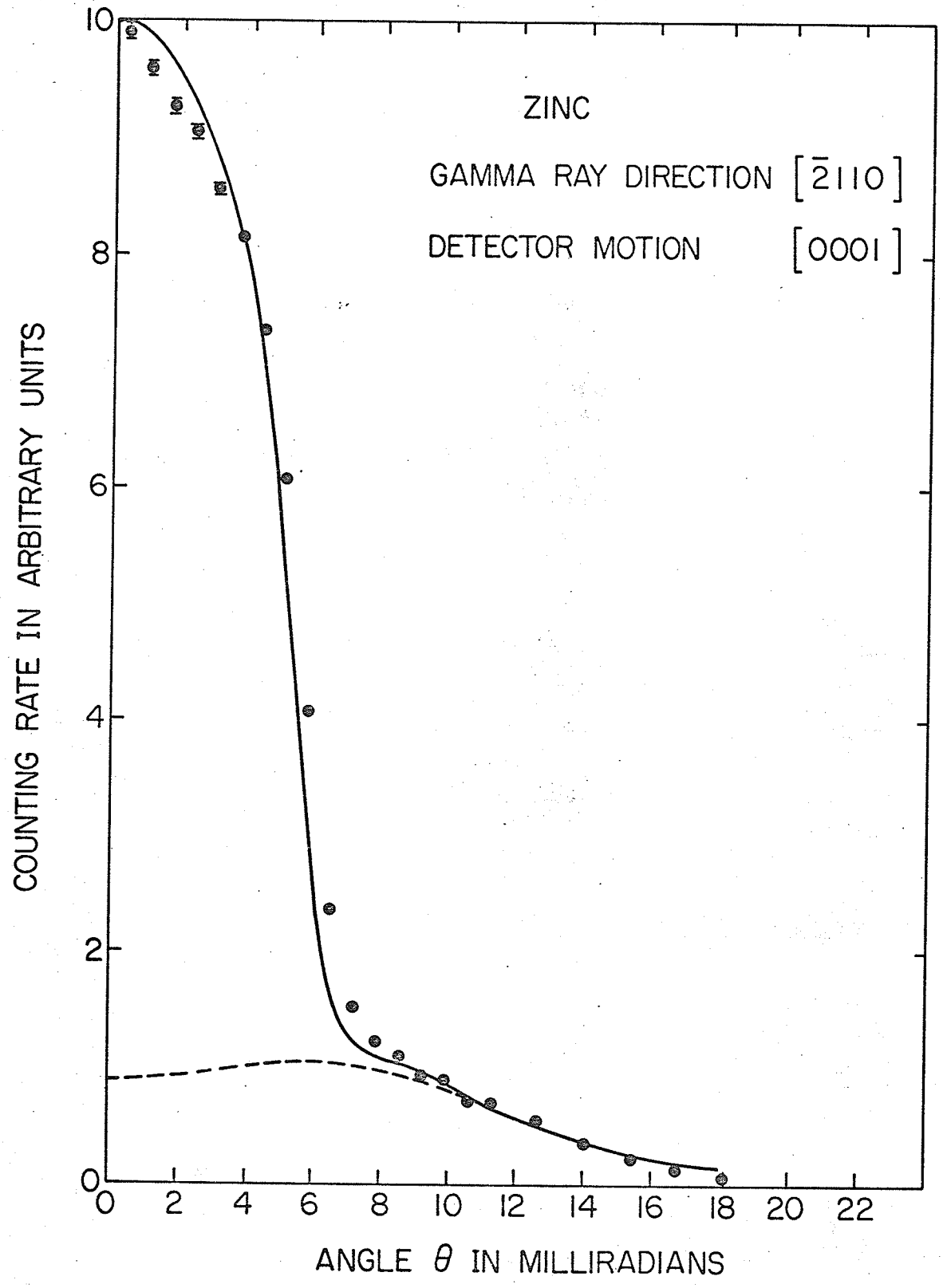

Figure 21. Zinc results with theoretical fit as calculated by method B. The dashed line is the calculated core contribution.

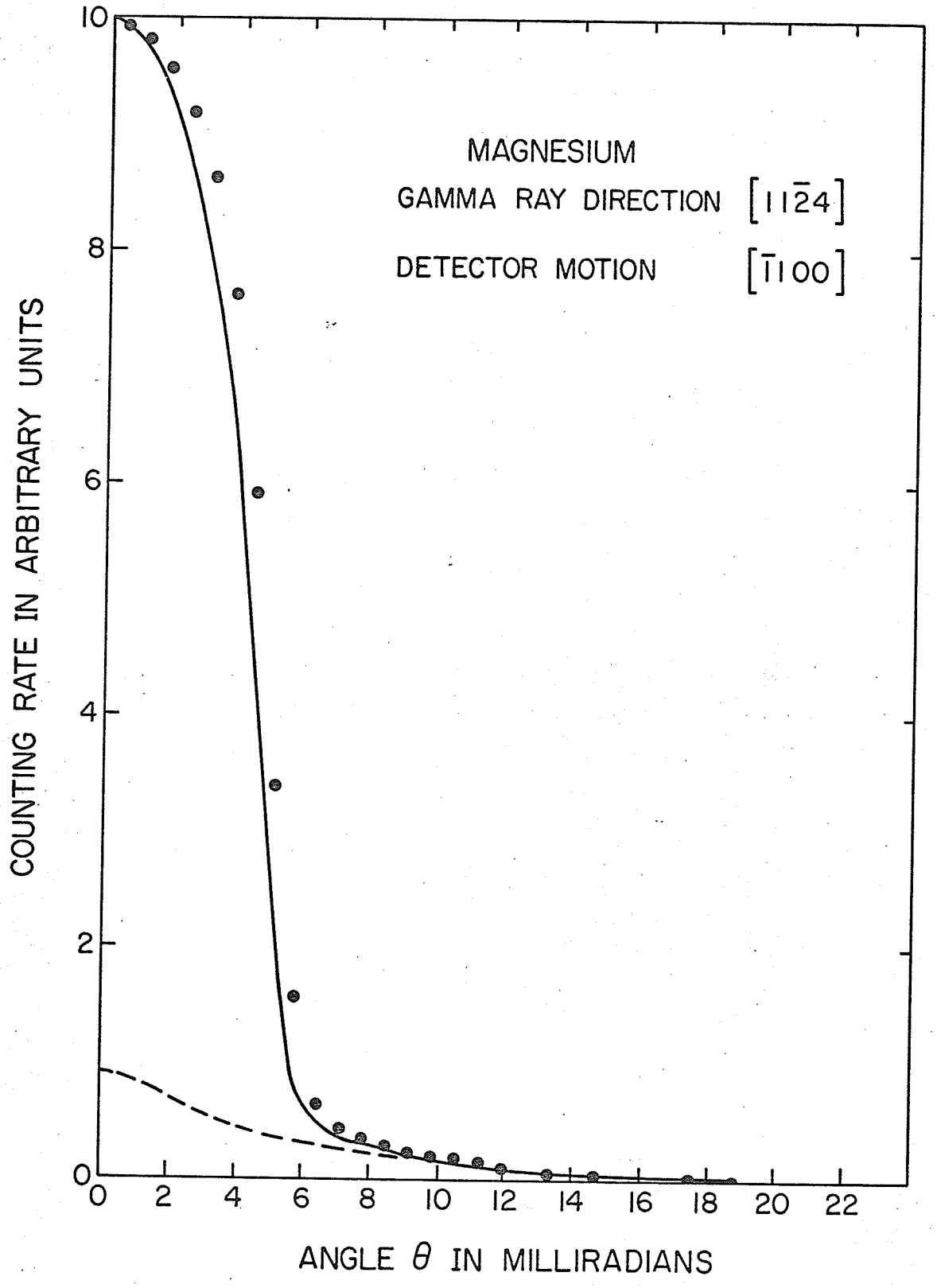

Figure 22. Magnesium results with theoretical fit as calculated by method A. The dashed line is the calculated core contribution.

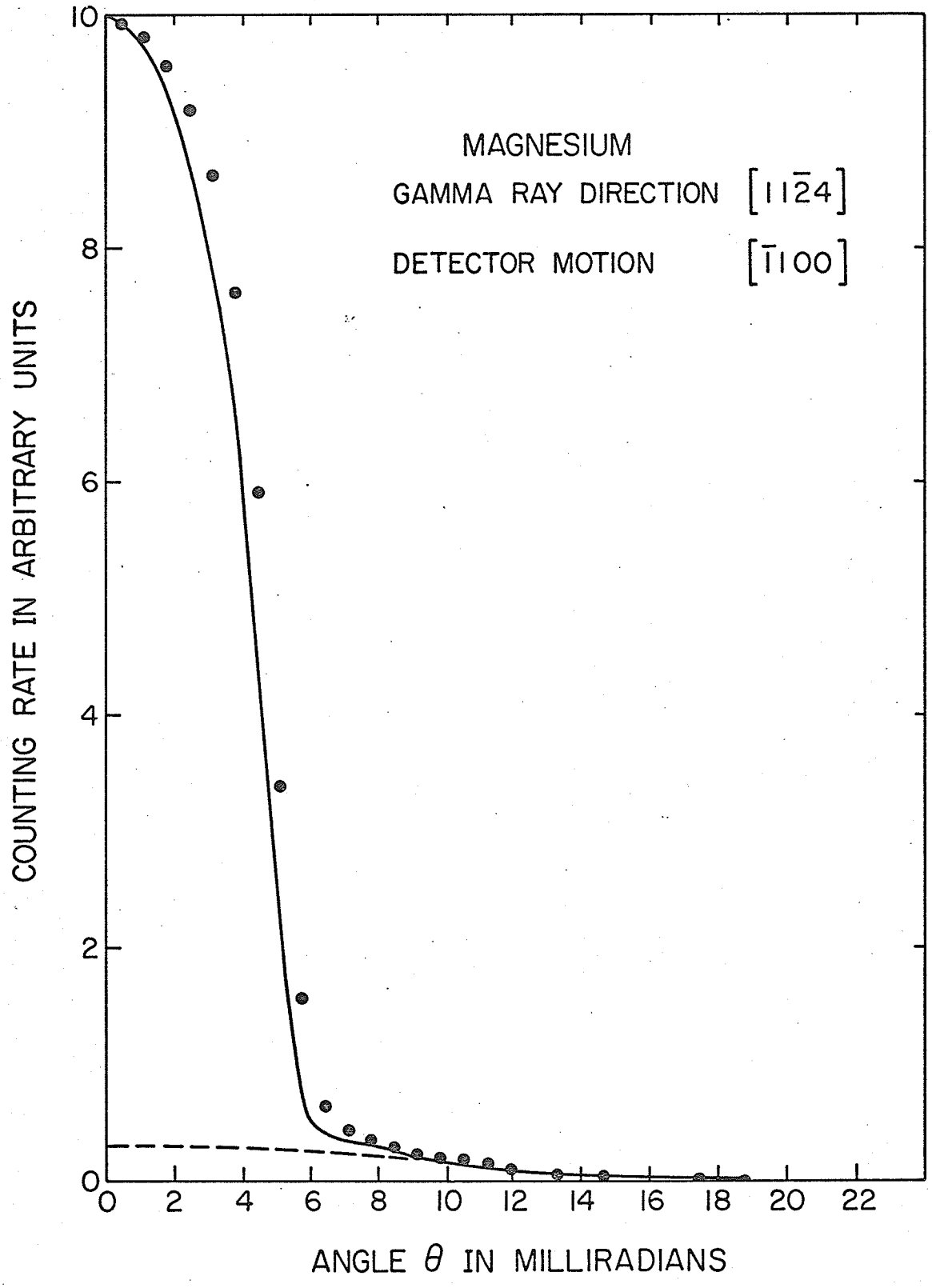

Figure 23. Magnesium results with theoretical fit as calculated by method B. The dashed line is the calculated core contribution.

Table II. Table of Fourier components of the positron wavefunction for zinc and magnesium.
($\Omega \sum_{\underline{G}} |a_{\underline{G}}|^2 = 1$. Ω is the volume of the unit cell.)

		(0000)	(0002)	$(2\bar{1}\bar{1}0)$	$(2\bar{1}\bar{1}1)$	$(2\bar{1}\bar{1}2)$
Zn	$\|a_{\underline{G}}\|^2$	0.0090	0.00014	0.000021	0.000028	0.0000014
Mg	$\|a_{\underline{G}}\|^2$	0.0060	0.000034	0.000014	0.000016	0.000006

fact, drop off slightly as θ approaches zero. This flatness results in a marginly better fit to the experimental data at small θ for the results of method B than for the results of method A. In the results for copper and magnesium, the fits obtained at large θ using either method are quite good. Since this is the region where most (if not all) of the annihilations are due to the core, this is where one would expect to get good agreement. Magnesium is not a very good test of the theory due to its very small core contribution. In the case of zinc, neither method gives a particularly good fit to the data at large θ.

Since a Wigner-Seitz type of calculation does not make use of the symmetry of the crystal, one might expect a poorer fit with a Wigner-Seitz positron wavefunction than with a crystal wavefunction. The fact that a better fit does result may imply that the fit obtained with method B was fortuitous. This is probably the case since the results obtained for cadmium in the long slit geometry indicate a considerable improvement in the fit when method A is used rather than method B (West et al, 1971). The averaging that occurs in the long slit geometry results in a smoother core distribution than that obtained in the point geometry and consequently a better fit at both small and large θ.

The similarity of the results for the three metals studied whose core electrons were assumed to be tightly bound indicates the sensitivity of the momentum distributions to the exact form of the positron wavefunction. This sensitivity is

likely to be present no matter how sophisticated the treatment of the electronic wavefunctions and will always limit an interpretation of the angular distribution in terms of the electronic structure.

In the case of copper, the lack of agreement in the intermediate core region ($\sim$5-10 mrad) can be attributed to a large extent to the inadequacy of the tight binding approximation. The 3d band in copper is affected somewhat by hybridization and one expects the Fermi electrons to have appreciable d character. In this case, it might be better to perform a complete "first principle" band calculation which would include s-d hybridization both for the "s" and the "3d" bands to obtain $\underline{k}$ dependent Fourier components. The zinc d band, on the other hand, is more tightly bound than that of copper and so the approximations used are more likely to be valid in this case. This is indicated by the smaller "residue" in the intermediate core region in the results for zinc compared with copper.

The results for zinc and magnesium are quite interesting since these metals are known to have zone-overlapping Fermi distributions. Berko and Plaskett (1958) have shown using nearly free electron theory that "humps" should be observed in the angular distributions at the zone faces. The present results for magnesium are consistent with the results of Berko (1962) which showed the nearly isotropic behavior of magnesium. The zinc results, however, indicate some structure at small θ in that the experimental points tend to fall below the theoretical curves in this region. Similar structure is also

evident in the work of Mogensen and Petersen (1971) on zinc in the long slit geometry. The direction of motion of the detectors was the same in both cases. The results in the latter case indicate that the experimental points for the single crystal sample fall below the experimental points for a polycrystalline sample of zinc. The zone face at π/c is not expected to contribute because of the expected vanishing energy gap at that face, but the zone face at $2\pi/c$ (4.9 mrad) may be giving rise to the observed structure. This is likely the case since the band gaps in zinc are known to be larger than the band gaps in magnesium (Reed and Brennert, 1963; Stark, 1967). A detailed theoretical calculation is obviously needed in order to correctly interpret the observed features in the zinc data.

It is worthwhile to point out that one must be careful when interpreting point detector results in terms of the topology of the Fermi surface. The present calculations assume no $\underline{k}$ dependence in the Fourier coefficients of the positron and electron wavefunctions. Inclusion of $\underline{k}$ dependence would result in a varying occupation density about each lattice point. Clearly the long slit geometry folds in much of the occupation density associated with higher momentum components whereas the point slit geometry does not and consequently results in a less accurate reflection of the Fermi surface.

Magnesium is a particularly interesting metal since its Fermi surface is so very nearly sperical (in the extended zone scheme). It is reasonable, therefore, to expect that

the enhancement factor for a free electron gas (Appendix I) can be used to improve the fit at intermediate angles. The enhancement factor for magnesium is (Kahana, 1963)

$$\varepsilon(\gamma) = 5.10 + 0.98\ \gamma^2 + 0.68\ \gamma^4 \qquad (4\text{-}1)$$

where $\gamma = P/k_F$. The results are shown in Figures 24 and 25. There is considerable improvement in the fit to the experimental points particularly for the results obtained with method B. This infers that the actual core distribution for magnesium must be fairly flat at small θ. It is clear that a better core calculation is necessary before the enhancement can be measured exactly.

It is very likely that the fits obtained for copper and zinc in particular can be improved by the use of enhancement factors. There are at present, however, no theoretical calculations which can be used to determine the effect of positron electron correlations in these metals.

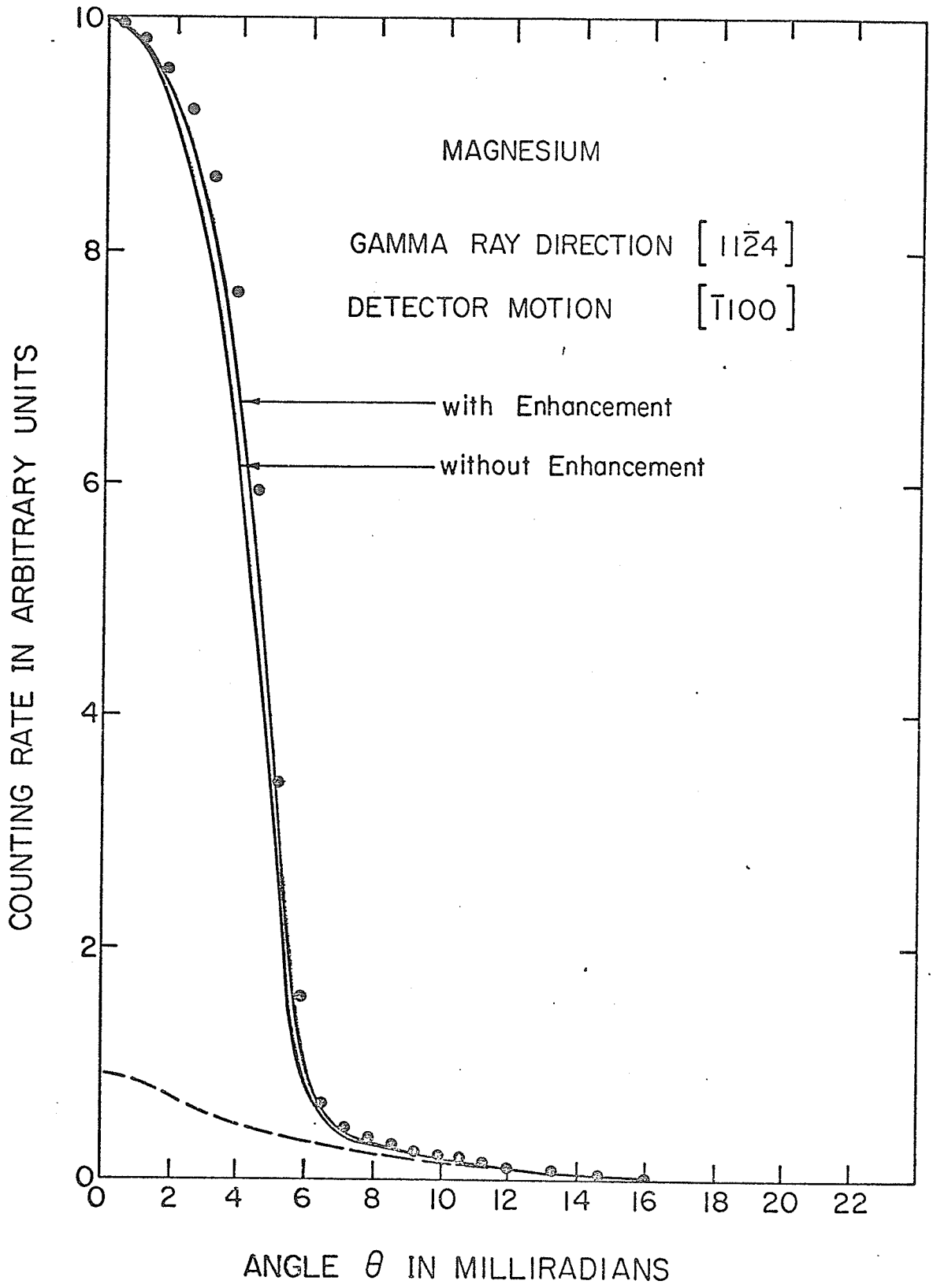

Figure 24. Magnesium results with the effect of enhancement included. The dashed line is the theoretical core as calculated by method A.

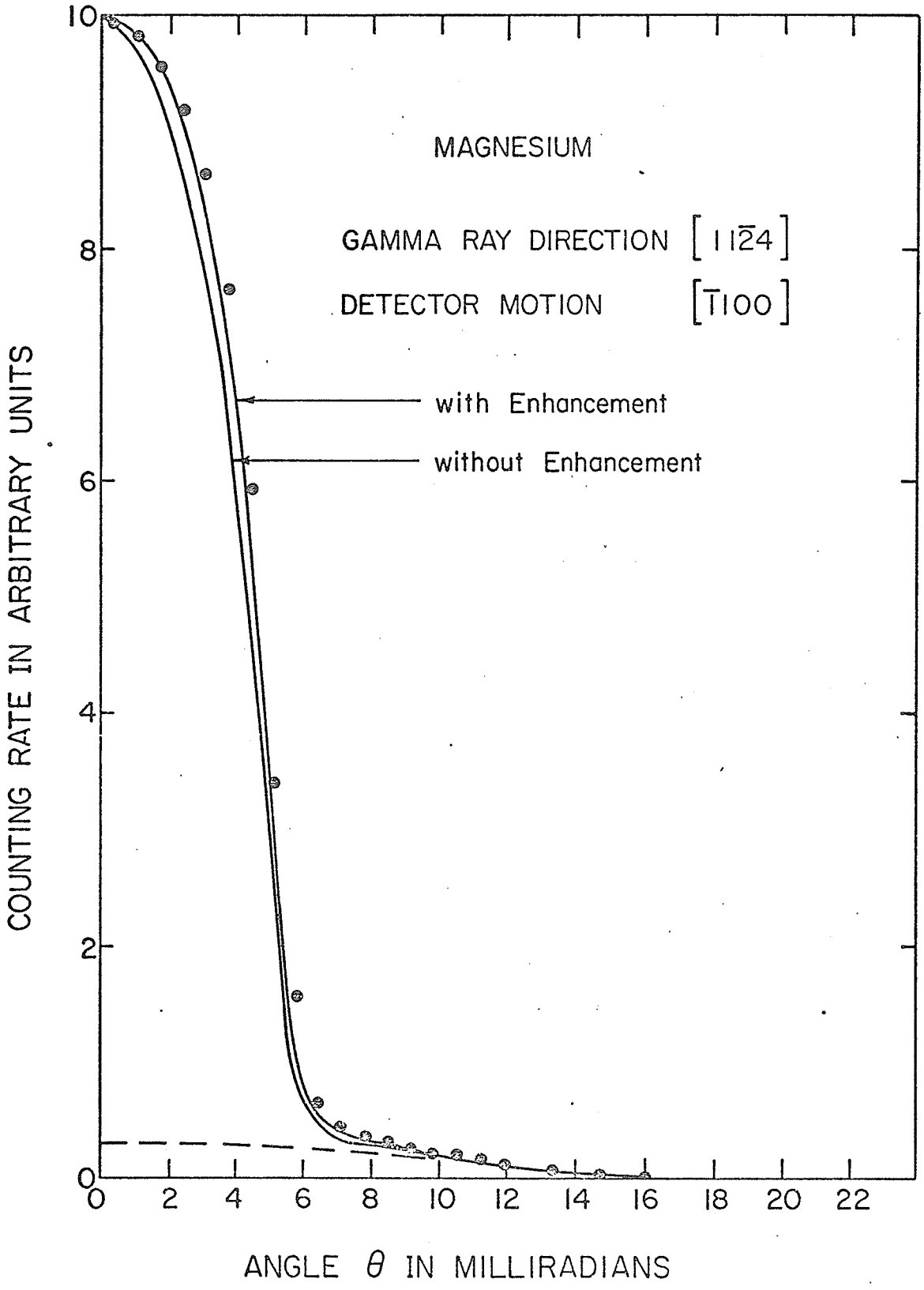

Figure 25. Magnesium results with the effect of enhancement included. The dashed line is the theoretical core as calculated by method B.

CHAPTER 5

CONCLUSIONS

From an experimental point of view, the aim of this thesis has been accomplished. A high resolution angular correlation apparatus has been constructed which is capable of studying all metals and alloys at coincidence counting rates that are about a factor of four higher than that obtained by any other apparatus of its kind known to the author. The present counting rate could easily be increased even more if suitable space could be found to accomodate an increase in the size of the apparatus. The usual restriction of the method to positron emitters has been lifted with the use of a novel source and sample arrangement. Several angular distributions have been measured to compare with theory.

From a theoretical point of view, however, the results are less than satisfying. The independent particle model seems to be a good first approximation to the experimental data but the discrepancies between the theoretical and experimental results are not easily accounted for. The angular correlations are very sensitive to the details of the positron and electron wavefunctions and this makes the interpretation of the data difficult.

A model which treats the core electrons as being

tightly bound and uses a positron wavefunction containing the crystal symmetry leads to a theoretical curve that gives a relatively good fit at high momenta. However, at low momenta the agreement is better when a Wigner-Seitz positron wavefunction is used. It is felt that the better agreement obtained with the Wigner-Seitz positron wavefunction is fortuitous and that further refinements to the positron and electron wavefunctions are necessary in order to obtain more realistic results.

The agreement between theory and experiment for a simple metal like magnesium is considerably improved by the use of an enhancement factor which accounts for positron electron correlations. It is felt that these correlations are important for all the metals studied and some account of them should be taken in the interpretation of the experimental data.

APPENDIX I

MANY-BODY EFFECTS

In a metal, the simplest picture is one where the positron annihilates with conduction electrons only. The positron is kept away from the positive ion sites in the metal as a result of its charge. Since the positron wave-function is nearly plane-wave-like except at the ion sites where it is zero, it can be approximated by a constant. This picture ignores all correlation effects and effects due to the crystal lattice. This is the Sommerfeld model of positron annihilation. The annihilation rate, originally derived by Dirac (1930) is given by

$$\lambda_{somm.} = \pi c r_0^2 n \text{ sec}^{-1}$$

where

r_0 = the classical electron radius

c = velocity of light

n = conduction electron density at the position of the positron

This can be rewritten in terms of a dimensionless parameter r_s given by

$$\frac{1}{n} = 4/3 \pi (a_0 r_s)^3$$

where a_0 is the Bohr radius, as

$$\lambda_{somm.} = 12 r_s^{-3} \times 10^9 \text{ sec}^{-1}$$

The values of $\lambda_{somm.}$ calculated in this way are consistently smaller than the experimental values. For example, the

calculated rate in sodium is about 36 times smaller than the experimentally observed rate. The observed rate is also quite independent of the electron density.

The independent particle model has succeeded in giving reasonably good agreement between theory and experiment as far as the general shape of the experimental curves are concerned and the observed detail in the curves seems to have physical significance. This same model, however, fails as well in predicting the lifetimes of positrons in metals. The predicted lifetimes are too long, and vary too much with electron density.

The reason for this lack of agreement is that both models ignore positron-electron correlations due to the strong Coulomb interaction. The annihilation rate depends on the electronic density at the positron in the independent particle model and this density is enhanced by pair correlations. In an electron gas, the Pauli exclusion principle prevents all states except those near the Fermi surface from being strongly affected by the positron. Only the electrons near the Fermi surface are able to move to screen the positron. Kahana (1963) has shown that the electron density at the positron is about 10 times the normal electron density in a metal.

It is, then, rather surprising that the independent particle model predicts the shape of the angular distributions as well as it does in view of such strong correlation effects.

As it turns out, more complete electron-gas calculations indicate that the annihilation probability can be described by the use of an enhancement factor that is large and rather weakly dependent on the electron momentum, especially for high density metals. This can be understood by considering the electron-electron interaction. If the positron-electron interaction is disregarded and the electron-electron interactions are taken fully into account, we get the result (Daniel and Vosko, 1960) that is the other extreme when compared to the calculations of Kahana (see Fig.24).

The interpretation is that the electrons are accompanied by screening clouds and the electron gas is regarded as an assembly of quasiparticles. The positron, however, is also accompanied by a screening cloud and the two clouds tend to cancel each other and the electron annihilates as a bare particle. The angular correlation then reflects the momentum distribution of bare electrons.

For further details of the many-body calculations that have been carried out, the reader is referred to the work of Kahana (1963), Carbotte and Kahana (1965), Zuchelli and Hickman (1964), Majumdar (1965), Carbotte (1967), Arponen and Jauho (1968), and Hatano et al (1965). These calculations have only treated the electron gas model. Carbotte (1966) has developed a many-body theory applicable to real metals for core annihilation. He obtains two terms, the usual term involving the electron-positron overlap integral and a second term, as important as the first, accounting for the

polarization of the ion core by the positron. The model is, however, too crude to give quantitative results.

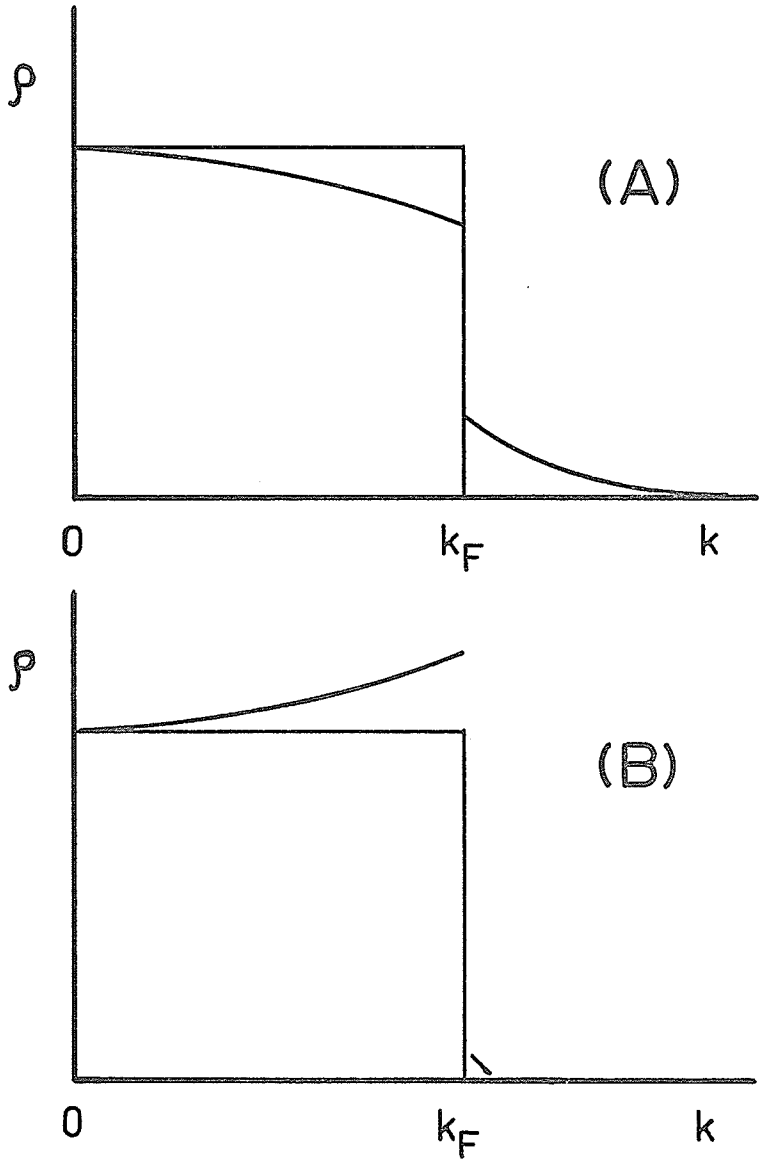

Figure 24. Schematic sketches of:

(A) Density in k-space of electrons compared with simple free electron theory (Daniel and Vosko, 1960).

(B) Density in k-space of electrons at the positron (Kahana, 1963).

APPENDIX II

THE RESOLUTION FUNCTION PROGRAM

```
FORTRAN IV G LEVEL 18                    MAIN                    DATE = 71074

0001                  DIMENSION COUNT(900)
0002                  REAL*8 DX2,DZ2,DY2,DX1,DZ1,DX,DY,DZ
0003                  DOUBLE PRECISION DTHET
0004                  DOUBLE PRECISION DAGE
0005                  DAGE=1.0
0006                  DY=142.0
0007                  DY2=-142.0
0008                  CF=1.0/16.0
0009                  AP=2.0/32.0
0010                  AI=3.0/32.0
0011                  AD=(1.0/16.0)**2
0012                  M=9
0013                  G=5.0
0014                  DO 1 J=1,900
0015                  COUNT(J)=0.0
0016             1    CONTINUE
0017                  DO 2 J=1,M
0018                  DO 2 JJ=1,M
0019                  DX2=((J-5)/G)*CD
0020                  DZ2=((JJ-5)/G)*CD
0021                  ADD=(DX2*DX2+DZ2*DZ2)
0022                  IF (ADD .GT. AD) GO TO 2
0023                  DO 5 K=1,M
0024                  DO 5 KK=1,M
0025                  DX=((K-5)/G)*CD
0026                  DZ=((KK-5)/G)*CD
0027                  ADD=(DX*DX+DZ*DZ)
0028                  IF (ADD .GT. AD) GO TO 5
0029                  DO 4 I=1,M
0030                  DO 4 II=1,M
0031                  DX1=((I-5)/G)*AP
0032                  DZ1=((II-5)/G)*AP
0033                  DTHET=((DX2-DX1)*(DX1-DX)+(DY2)*(-DY))/
                     1((DSQRT((DX2-DX1)**2+(DY2)**2))*(DSQRT((DX1-
                     2DX)**2+(-DY)**2)))
0034                  ZE=(DACOS(DTHET))*1.0E+04
0035                  IJ=IFIX(ZE)
0036                  IJ=IJ+1
0037                  COUNT(IJ)=COUNT(IJ)+1.0
0038             4    CONTINUE
0039             5    CONTINUE
0040             2    CONTINUE
0041                  DO 3 K=1,50
0042                  WRITE(6,101) COUNT(K)
0043           101    FORMAT(5(1X,E15.6))
0044             3    CONTINUE
0045                  CALL EXIT
0046                  END
```

APPENDIX III

THE TIME INDEPENDENT ANGULAR CORRELATION PROGRAM

```
FORTRAN IV G LEVEL 19                MAIN                DATE = 71141          10/41/45

0001                 DIMENSION AT(1000),BT(1000),ANREL(1000),ARAT(1000),
                    1BNREL(1000),C(30,30),CORRAT(50)
0002                 I=0
0003                 ACCUR=0.0
0004                 ALAM=0.693/(12.7*60.0)
0005                 TAU1=(37.0E-09)/60.0
0006                 TAU2=(19.0E-09)/60.0
0007                 TAU3=(58.0E-09)/60.0
0008                 TAU4=(43.0E-09)/60.0
0009                 S1=290.0*60.0
0010                 S11=290.0*60.0
0011                 S2=340.0*60.0
0012                 S22=270.0*60.0
0013                 S3=380.0*60.0
0014                 S33=230.0*60.0
0015                 S4=351.0*60.0
0016                 S44=250.0*60.0
0017          9      CONTINUE
0018                 I=I+1
0019                 READ(5,10) AT(I),BT(I)
0020          10     FORMAT(F12.3,4X,F12.3)
0021                 IF(AT(I) .GT. 0.0) GO TO 9
0022                 NN=I-1
0023                 DO 7 I=1,NN
0024                 BS=(EXP(-2.0*ALAM*AT(I))-EXP(-2.0*ALAM*BT(I)))/ALAM
0025                 BS=(TAU1*S1*S11+TAU2*S2*S22+TAU3*S3*S33+TAU4*S4*S44)*BS
0026                 WRITE(6,803) BS
0027          803    FORMAT(E16.8)
0028                 IF(I .GT. 5) COUNT=100.
0029                 IF(I .LE. 5) COUNT=200.
0030                 IF(I .GT. 300) COUNT=100.
0031                 ANREL(I)=COUNT-BS
0032                 ACCUR=ACCUR+ANREL(I)
0033          7      CONTINUE
0034                 DO 17 I=1,NN
0035                 ARAT(I)=(ANREL(I)/ANREL(1))*((EXP(-ALAM*AT(1))-EXP(-ALAM*BT(1)))
                    1/(EXP(-ALAM*AT(I))-EXP(-ALAM*BT(I))))
0036                 WRITE(6,804) AT(I),BT(I),ARAT(I)
0037          804    FORMAT(F12.3,4X,F12.3,9X,E16.5)
0038          17     CONTINUE
0039                 ISTOP=+3
0040                 ISTART=15
0041                 NNN=ISTART-ISTOP
0042                 NNN=IABS(NNN)
0043                 K=0
0044                 J=0
0045          37     CONTINUE
0046                 J=J+1
0047                 LL=J
0048                 KJ=K
0049                 IJ=((J-1)/2)*2+1
0050                 IJ=IJ-J
0051                 DO 27 I=1,NNN
0052                 IF (IJ .EQ. 0) K=K+1
0053                 IF (IJ .LT. 0) K=KJ+NNN-I+1
0054                 C(I,J)=ARAT(K)
0055                 WRITE(6,803) C(I,J)
0056          27     CONTINUE
```

```
FORTRAN IV G LEVEL  19                    MAIN                    DATE = 71141

0057                L=(NNN*J)+NNN
0058                K=NNN*J
0059                IF(L .LT. NN) GO TO 37
0060                M=0
0061                DO 48 K=1,LL
0062                BNREL(K)=0.0
0063                DO 47 I=1,NNN
0064                M=M+1
0065                BNREL(K)=BNREL(K)+AMREL(M)
0066          47    CONTINUE
0067                WRITE(6,803) BNREL(K)
0068          48    CONTINUE
0069                DO 51 I=1,NNN
0070                CORRAT(I)=0.0
0071                DO 52 J=1,LL
0072                CORRAT(I)=CORRAT(I)+C(I,J)*BNREL(J)
0073          52    CONTINUE
0074                WRITE(6,803) CORRAT(I)
0075          51    CONTINUE
0076                AB=CORRAT(1)
0077                DO 43 I=1,NNN
0078                CORRAT(I)=CORRAT(I)/AB
0079          43    CONTINUE
0080                WRITE(6,55)(CORRAT(I),I=1,NNN)
0081          55    FORMAT(F15.5)
0082                ACCUR=ACCUR/NNN
0083                WRITE(6,55) ACCUR
0084                CALL EXIT
0085                END
```

APPENDIX IV

THE CONDUCTION ELECTRON

ANGULAR DISTRIBUTION PROGRAM

```
FORTRAN IV G LEVEL  20.1              MAIN              DATE = 72026          11/51/41          PI75

0001                  DIMENSION S(81,81),SI(81,81)
0002                  DIMENSION F1(21,21),F2(21,21),F3(21,21),F4(21,21),ALFA(8)
0003                  DIMENSION X5(8),Y5(8),Z5(8),XP(8),YP(8),ZP(8)
0004                  M7=81
0005                  D=0.78
                C     COMMENT D= FERMI SPHERE RADIUS
0006                  THI=-((3.14)/4.0)
0007                  THE=-(3.14)*(54.7/180.0)
                C     COMMENT ROTATE Z' AXIS ALONG GAMMA RAY
                C     COMMENT ROTATE X' AXIS ALONG XTAL AXIS
0008                  PSI=0.0
0009                  THICOS=COS(THI)
0010                  THECOS=COS(THE)
0011                  PSICOS=COS(PSI)
0012                  THISIN=SIN(THI)
0013                  THESIN=SIN(THE)
0014                  PSISIN=SIN(PSI)
0015                  R=0.162
0016                  AL=0.086
                C     COMMENT R AND AL DETERMINE NECK SIZE
0017                  X5(1)=1
0018                  X5(2)=-1
0019                  X5(3)=1
0020                  X5(4)=1
0021                  Y5(1)=+1
0022                  Y5(2)=+1
0023                  Y5(3)=-1
0024                  Y5(4)=+1
0025                  Z5(1)=1
0026                  Z5(2)=1
0027                  Z5(3)=1
0028                  Z5(4)=-1
0029                  DO 300 I=1,4
0030                  XP(I)=X5(I)*(PSICOS*THICOS-THECOS*THISIN*PSISIN)+Y5(I)*(PSICOS
                     1*THISIN+THECOS*THICOS*PSISIN)+Z5(I)*(PSISIN*THESIN)
0031                  YP(I)=X5(I)*(-PSISIN*THICOS-THECOS*THISIN*PSICOS)+Y5(I)*(-PSISIN
                     1*THISIN+THECOS*THICOS*PSICOS)+Z5(I)*(PSICOS*THESIN)
0032                  ZP(I)=X5(I)*(THESIN*THISIN)+Y5(I)*(-THESIN*THICOS)+Z5(I)*THECOS
0033                  WRITE(6,4) XP(I),YP(I),ZP(I)
0034                  PCOS=(XP(I)**2+YP(I)**2)/((SQRT(XP(I)**2+YP(I)**2+ZP(I)**2))
                     1*(SQRT(XP(I)**2+YP(I)**2)))
0035                  ALFA(I)=ARCOS(PCOS)
0036                  WRITE(6,4) ALFA(I)
                C     COMMENT ALFA AIS ANGLE OF NECKS TO X'Y' PLANE
0037                  M7=I+4
0038                  XP(M7)=-XP(I)
0039                  YP(M7)=-YP(I)
0040                  ZP(M7)=-ZP(I)
0041                  ALFA(M7)=ALFA(I)
0042                  DO 301 II=1,21
0043                  XI=II
0044                  R=((XI-11.0)/10.0)*0.25
0045                  TRI=(R*R-P*P)
0046                  DO 302 JJ=1,21
0047                  DIFF=0.0
0048                  IF( TRI .LT. 0.0) GO TO 303
0049                  RHO=2.0*(SQRT(TRI))
0050                  XJ=JJ
```

C

```
FORTRAN IV G LEVEL  20.1          MAIN          DATE = 72026      11/51/41      P1

0051                A1X=((XJ-11.0)/10.0)*0.25
0052                A11X=ABS(A1X)
0053                A3=COS(ALFA(I))*(AL/2.0)+(RHO/2.0)*SIN(ALFA(I))
0054                IF(A11X .GT. A3) GO TO 303
0055                A1Y=(-1.0/TAN(ALFA(I)))*A1X+AL/(2.0*SIN(ALFA(I)))
0056                A2Y=TAN(ALFA(I))*A1X+RHO/(2.0*COS(ALFA(I)))
0057                AY=A1Y
0058                IF(A2Y .LT. A1Y) AY=A2Y
0059                A3Y=(-1.0/TAN(ALFA(I)))*A1X-AL/(2.0*SIN(ALFA(I)))
0060                A4Y=(TAN(ALFA(I)))*A1X-RHO/(2.0*COS(ALFA(I)))
0061                BY=A3Y
0062                IF(A4Y .GT. A3Y) BY=A4Y
0063                DIFF=ABS(AY-BY)
0064          303   CONTINUE
0065                IF(I .EQ. 1) E1(II,JJ)=DIFF
0066                IF(I .EQ. 2) E2(II,JJ)=DIFF
0067                IF(I .EQ. 3) E3(II,JJ)=DIFF
0068                IF(I .EQ. 4) E4(II,JJ)=DIFF
0069          302   CONTINUE
0070          301   CONTINUE
0071          300   CONTINUE
              C     COMMENT NECK ALONGS IF PROJECTED ALONG Y OR J AXIS
              C     COMMENT COORD SYSTEM RIGHT HANDED SAME AS BASE OF 3-D SYSTEM
0072                DO 305 I=1,21
0073          305   WRITE(6,306) (E1(I,J),J=1,21)
0074          306   FORMAT(21E5.3)
0075                DO 501 I=1,21
0076          501   WRITE(6,306) (E2(I,J),J=1,21)
0077                DO 1 JA=1,NZ
0078                DO 2 JB=1,NZ
0079                XA=JA
0080                XB=JB
              C     COMMENT THIS SECTION CALC PROJECT OF SPHERE IN X'Y' PLANE
0081                X1=((XA-41)/20)*(0.5)
0082                Y1=((XB-41)/20)*(0.5)
0083                TRI=(0*0-X1*X1-Y1*Y1)
0084                IF(TRI .LT. 0.0) TRI=0.0
0085                Z1=SQRT(TRI)
              C     COMMENT COULD HERE COMPLICATE SURFACE
0086                DIFF=2.0*Z1
0087                S(JA,JB)=DIFF
0088          2     CONTINUE
0089          1     CONTINUE
0090                DO 403 N5=1,3
              C     COMMENT THIS SECTION ADDS PROJECTION OF NECKS TO PROJECT SPHERE
0091                ALEN=(0+(AL/2.0))*COS(ALFA(N5))
0092                BLEN=SQRT(XP(N5)**2+YP(N5)**2)
0093                AXP=XP(N5)*(ALEN/BLEN)
0094                AYP=YP(N5)*(ALEN/BLEN)
0095                SIGCOS=AYP/(SQRT(AXP*AXP+AYP*AYP))
0096                SIGSIN=AXP/(SQRT(AXP*AXP+AYP*AYP))
0097                DO 401 M2=1,21
0098                DO 402 N2=1,21
0099                X9=N2
0100                Y9=M2
0101                Y6=((Y9-11.0)/10.0)*0.25
0102                X6=((X9-11.0)/10.0)*0.25
0103                X7=X6*SIGCOS-Y6*SIGSIN
```

```
0104                  Y7=X6*SIGSIN+Y6*SIGCOS
0105                  X7=X7+AXP
0106                  Y7=Y7+AYP
0107                  M3=IFIX(40.0*X7)+41
0108                  M3=IFIX(40.0*Y7)+41
0109                  IF(M3 .LT.  1) GO TO 402
0110                  IF(M3 .LT.  1) GO TO 402
0111                  IF(M3 .GT. MZ) GO TO 402
0112                  IF(M3 .GT. MZ) GO TO 402
0113                  IF(N5 .EQ. 1) S(N3,M3)=S(N3,M3)+E1(N2,M2)
0114                  IF(N5 .EQ. 2) S(N3,M3)=S(N3,M3)+E2(N2,M2)
0115                  IF(N5 .EQ. 3) S(N3,M3)=S(N3,M3)+E3(N2,M2)
0116                  IF(N5 .EQ. 4) S(N3,M3)=S(N3,M3)+E4(N2,M2)
0117                  IF(N5 .EQ. 5) S(N3,M3)=S(N3,M3)+E1(N2,M2)
0118                  IF(N5 .EQ. 6) S(N3,M3)=S(N3,M3)+E2(N2,M2)
0119                  IF(N5 .EQ. 7) S(N3,M3)=S(N3,M3)+E3(N2,M2)
0120                  IF(N5 .EQ. 8) S(N3,M3)=S(N3,M3)+E4(N2,M2)
0121            402   CONTINUE
0122            401   CONTINUE
0123            403   CONTINUE
0124                  DO 405 I=1,MZ
0125                  DO 405 J=1,MZ
0126                  S1(I,J)=S(I,J)*0.912
                C     COMMENT THE ABOVE TERM IS COMPONENT OF POSITRON WAVEFUNCTION
0127            405   CONTINUE
0128                  DO 3 I=1,14
0129                  READ(5,4) XK,YK,ZK
0130            4     FORMAT(3F15.3)
0131                  WRITE(6,4) XK,YK,ZK
0132                  XK1=(PSICOS*THICOS-THECOS*THISIN*PSISIN)*XK+(PSICOS*THISIN+
                     1THECOS*THICOS*PSISIN)*YK+(PSISIN*THESIN)*ZK
0133                  YK1=(-PSISIN*THICOS-THECOS*THISIN*PSICOS)*XK+(-PSISIN*THISIN
                     1+THECOS*THICOS*PSICOS)*YK+(PSICOS*THESIN)*ZK
0134                  WRITE(6,4) XK1,YK1,ZK
0135                  I1=IFIX(40.0*XK1)
0136                  I2=IFIX(40.0*YK1)
0137                  DO 5 JA=1,MZ
0138                  DO 6 JB=1,MZ
0139                  IA=JA+I1
0140                  IB=JB+I2
0141                  IF(IA .GT. MZ) GO TO 6
0142                  IF (IA .LT. 1) GO TO 6
0143                  IF(IB .GT. MZ) GO TO 6
0144                  IF(IB .LT. 1) GO TO 6
                C     COMMENT WEIGH TERMS ARE HMC IN POSITRON WAVEFUNCTION
0145                  WEIGH=.040/6.0
0146                  VEC=(XK*XK+YK*YK+ZK*ZK)
0147                  IF(VEC .LT. 3.5) WEIGH=0.144/8.0
0148                  S1(IA,IB)=S1(IA,IB)+(S(JA,JB)*WEIGH)
0149            6     CONTINUE
0150            5     CONTINUE
0151            3     CONTINUE
0152                  DO 51 K=1,81
0153            51    WRITE(6,201) (S1(K,L),L=1,25)
0154            201   FORMAT('0',25F5.3)
0155                  DO 52 K=1,81
0156            52    WRITE(6,201) (S1(K,L),L=26,50)
0157            202   FORMAT('0',16F5.3)
```

C

0172

FORTRAN IV G LEVEL 20.1 MAIN DATE = 72026

```
0158                    ANO=1.0
0159                    BNO=56.
0160                    I=41
0161                    DO 901 J=1,NZ
0162                    VAC=0.0
0163                    DO 902 I1=1,15
0164                    DO 903 J1=1,15
0165                    I11=I1-8
0166                    J11=J1-8
0167                    I2=I+I11
0168                    J2=J+J11
0169                    IF(I2 .GT. NZ) GO TO 903
0170                    IF(J2 .GT. NZ) GO TO 903
0171                    IF(J2 .LT.  1) GO TO 903
0172                    IF(I2 .LT.  1) GO TO 903
0173                    U=I11*(1.0/40.0)
0174                    V=J11*(1.0/40.0)
0175                    DAS=SQRT(U*U+V*V)
0176                    RES=ANO*(EXP(-BNO*DAS*DAS))
0177                    IF(DAS .GT. .175) RES=0.0
0178                    VAC=VAC+S1(I2,J2)*RES
0179            903     CONTINUE
0180            902     CONTINUE
0181                    WRITE(6,904) VAC
0182            904     FORMAT(F16.5)
0183            901     CONTINUE
0184                    CALL EXIT
0185                    END
```

APPENDIX V

THE FOLDING OF THE EXPERIMENTAL RESOLUTION INTO THE THEORETICAL CORE ELECTRON ANGULAR DISTRIBUTION

FORTRAN IV G LEVEL 19 MAIN DATE = 71286

```
0001                DIMENSION VEC1(15)
0002                SLOP1=.0975
0003                CEPT1=.81
0004                SLOP2=.03
0005                CEPT2=.53
0006                H=1.23
0007                X=-1.0
0008                DD=(4.0/5.0)*2.0
0009                DO 1 I=1,10
0010                X=X+1.0
0011                VEC1(I)=0.0
0012                DO 2 J=1,9
0013                AJ=J
0014                DO 3 K=1,9
0015                AK=K
0016                X1=(((5.0-AJ)/5.0)*2.0)
0017                Y1=(((5.0-AK)/5.0)*2.0)
0018                D1=SQRT(X1*X1+Y1*Y1)
0019                IF (D1 .GT. DD) GO TO 3
0020                X1=X1+X
0021                D=SQRT(X1*X1+Y1*Y1)
0022                IF (D .LT. 4.0) Y=-SLOP1*D+CEPT1
0023                IF(D .GT. 4.0) Y=-SLOP2*D+CEPT2
0024                RES=1.0*EXP(-H*D1*D1)
0025                VEC=RES*Y
0026                VEC1(I)=VEC1(I)+VEC
0027          3     CONTINUE
0028          2     CONTINUE
0029                WRITE(6,4) VEC1(I),X
0030          4     FORMAT(2E16.8)
0031          1     CONTINUE
0032                CALL EXIT
0033                END
```

BIBLIOGRAPHY

Anderson, C.D., (1933), Phys. Rev., 43, 491.

Arponen, J., and Juaho, P., (1968), Phys. Rev., 167, 239.

Becker, E.H., (1969), unpublished data.

Berko, S., Kelly, R.E., and Plaskett, J.S., (1957), Phys. Rev., 106, 824.

Berko, S., and Plaskett, J.S., (1958), Phys. Rev., 110, 1062.

Berko, S., (1962), Phys. Rev., 128, 2166.

Berko, S., Cushner, S., and Erskine, J.C., (1968), Phys. Letters, 27A, 668.

Carbotte, J.P., and Kahana, S., (1965), Phys. Rev., 139, 213.

Carbotte, J.P., (1966), Phys. Rev., 144, 309.

Carbotte, J.P., (1967), Phys. Rev., 155, 197.

Carbotte, J.P., and Arora, H.L., (1967), Can. J. Phys., 45, 387.

Colombino, P., Fiscella, B., and Trossi, L., (1963), Nuovo Cimento, 27, 589.

Colombino, P., Fiscella, B., and Trossi, L., (1964), Nuovo Cimento, 31, 950.

Conners, D.C., Crisp, V.H.C., and West, R.N., (1970), Phys. Letters, 33A, 180.

Coussot, G., (1971), Phys. Rev., B3, 1048.

Cushner, S., Erskine, J.C., and Berko, S., (1970), Phys. Rev., B1, 2852.

Daniel, E., and Vosko, S.H., (1960), Phys. Rev., 120, 2041.

DeBenedetti, S., Cowan, C.E., Konneker, W.R., and Primakoff, H., (1950), Phys. Rev., 77, 205.

Deutsch,M., (1951), Phys. Rev., 82, 455.

Dirac, P.A.M., (1930), Proc. Cambridge Phil. Soc., 26, 361.

Donaghy, J.J., and Stewart, A.T., (1967), Phys. Rev., 164, 391.

Fabian, D.J., (1968), Soft X Ray Band Spectra and the Electronic Structure of Materials, Academic Press, New York.

Ferrell, R.A., (1956), Rev. Mod. Phys., 28, 308.

Fujiwara, K., (1965), J. Phys. Soc. Japan, 20, 1533.

Fujiwara, K., and Sueoka, O., (1966), J. Phys. Soc. Japan, 21, 1947.

Fujiwara, K., Sueoka, O., and Imura, T., (1966), J. Phys. Soc. Japan, 21, 2738.

Fujiwara, K., and Sueoka, O., (1967), J. Phys. Soc. Japan, 23, 1242.

Garwin, R.L., (1953), Phys. Rev., 91, 1571.

Gould, A.G., (1971), Private communication.

Gupta, R.P., and Loucks, T.L., (1968), Phys. Rev., 176, 848.

Hatano, A., Kanazawa, H., and Mizuno, Y., (1965), Progr. Theoret. Phys. (Kyoto), 34, 875.

Herman, F., and Skillman, S., (1963), Atomic Structure Calculations, Prentice Hall.

Hotz, H.P., Mathiesen, J.M., and Hurley, J.P., (1968), Phys. Rev., 170, 351.

Kahana, S., (1963), Phys. Rev., 129, 1622.

Lang, G., and DeBenedetti, S., (1957), Phys. Rev., 108, 914.

Lee-Whiting, G.E., (1955), Phys. Rev., 97, 1557.

Loucks, T.L., (1966), Phys. Rev., 144, 504.

Majumdar, C.K., (1965), Phys. Rev., 140, 227.

McAlister, A.J., Stern, E.A., and McGroddy, J.C., (1965), Phys. Rev., 140, A2105.

Melngailis, J., and DeBenedetti, S., (1966), Phys. Rev., 145, 400.

Mijnarends, P.E., (1967), Phys. Rev., 160, 512.

Mijnarends, P.E., (1969), Phys. Rev., 178, 622.

Mogensen, O., and Petersen, K., (1969), Phys. Letters, 30A, 542.

Mogensen, O.E., and Trumpy, G., (1969), Phys. Rev., 188, 639

Mohorovicic, S., (1934), Astron, Nacht, 253, 94.

Murray, B.W., and McGervey, J.D. (1970), Phys. Rev. Letters, 24, 9.

Phillips, W.C., and Weiss, R.J., (1969), Phys. Rev., 182, 923.

Reed, W.A., and Brennert, G.F., (1963), Phys. Rev., 130, 565.

Ruark, A.E., (1945), Phys. Rev., 68, 278.

Shand, J.B., (1969), Phys. Letters, 30A, 478.

Stachowiak, H., (1970), Phys. Stat. Sol., 41, 599.

Stark, R.W., (1967), Phys. Rev., 162, 589.

Stedman, R., and Nilsson, G., (1965), Phys. Rev. Letters, 15, 634.

Stewart, A.T., (1957), C. J. Phys., 35, 168.

Stewart, A.T., Shand, J.B., Donaghy, J.J., and Kusmiss, J.H., (1962), Phys. Rev., 128, 118.

Stewart, A.T., and Shand, J.B., (1966), Phys. Rev. Letters, 16, 261.

Stewart, A.T., Shand, J.B., and Kim, S.M., (1966), Proc. Phys. Soc., 88, 1001.

Stewart, A.T., and Roellig, L.O., (1967), Positron Annihilation, Academic Press, New York.

Strominger, D., Horlander, J.M., Seaborg, G.T., (1958), Rev. Mod. Phys., 30, 585.

Stroud, D., and Ehrenreich, H., (1968), Phys. Rev., 171, 399.

Sueoka, O., (1967), J. Phys. Soc. Japan, 23, 1246.

Wallace, P.R., (1960), in Solid State Physics, Academic Press, New York.

West, R.N., Gould, A.G., and Hogg, B.G., (1971), to be published.

Williams, D.L., Petijevich, P., and Jones, G., (1965), Bull. Amer. Phys. Soc., 10, 1181.

Williams, D.L., Becker, E.H., Petijevich, P., and Jones, G., (1968), Phys. Rev. Letters, 20, 448.

Williams, R.W., Loucks, T.L., and Mackintosh, A.R., (1966), Phys. Rev. Letters, 16, 168.

Zuchelli, A.J., and Hickman, T.G., (1964), Phys. Rev., 136, A1728.